Combining GW calculations with exact-exchange density-functional theory: An analysis of valence-band photoemission for compound semiconductors

Patrick Rinke[1], **Abdallah Qteish**[1,2], **Jörg Neugebauer**[1,3,4], **Christoph Freysoldt**[1] **and Matthias Scheffler**[1]

[1] Fritz-Haber-Institut der Max-Planck-Gesellschaft, D-14195 Berlin-Dahlem, Germany

[2] Department of Physics, Yarmouk University, 21163-Irbid, Jordan

[3] Department of Theoretical Physics, University of Paderborn, D-33095 Paderborn, Germany

[4] Max-Planck-Institut für Eisenforschung, Department of Computational Materials Design, D-40237 Düsseldorf, Germany

E-mail: `rinke@fhi-berlin.mpg.de`

Abstract. We report quasiparticle-energy calculations of the electronic bandstructure as measured by valence-band photoemission for selected II-VI compounds and group-III-nitrides. By applying GW as perturbation to the ground state of the fictitious, non-interacting Kohn-Sham electrons of density-functional theory (DFT) we systematically study the electronic structure of zinc-blende GaN, ZnO, ZnS and CdS. Special emphasis is put on analysing the role played by the cation semicore d-electrons that are explicitly included as valence electrons in our pseudopotential approach. Unlike in the majority of previous GW studies, which are almost exlusively based on ground state calculations in the local-density approximation (LDA), we combine GW with exact-exchange DFT calculations in the optimised-effective potential approach (OEPx). This is a much more elaborate and computationally expensive approach. However, we show that applying the OEPx approach leads to an improved description of the d-electron hybridisation compared to the LDA. Moreover we find that it is essential to use OEPx pseudopotentials in order to treat core-valence exchange consistently. Our OEPx based quasiparticle valence bandstructures are in good agreement with available photoemission data in contrast to the ones based on the LDA. We therefore conclude that for these materials OEPx constitutes the better starting point for subsequent GW calculations.

Contents

1. Introduction

From the discovery of the photo-electric effect in the early days of the 20th century photo-electron spectroscopy has developed into an invaluable experimental method for the study of electron excitations in bulk solids and surfaces. Photoemission spectroscopy (PES) [1, 2, 3] and its inverse counterpart (IPES) [4, 5, 6] have been instrumental for our current understanding of elementary excitation processes in condensed matter and for deciphering the electronic structure of many materials. The success of PES and IPES ows much to the interpretation of the photo-electron spectra in terms of single-particle excitations or *quasiparticles* in the language of many-body quantum-mechanics.

In the first part of this article we will briefly recapitulate this connection between photo-electron spectroscopy of delocalised valence states and Green's function theory and illustrate how angular resolved (I)PES spectra can be interpreted in terms of the quasiparticle bandstructure. Within the theoretical framework of many-body perturbation theory we employ Hedin's *GW* approximation [7] to calculate the quasiparticle energy spectrum, where *G* refers to the Green's function and *W* to the dynamically screened Coulomb interaction. The *GW* method and the computational details of the bandstructure calculations from the state-of-the-art (based on the local-density-approximation) to recent developments (optimised effective potential method to density-functional theory) will be introduced in more detail later. For further reading with regard to the connection between photo-electron spectroscopy and many-body perturbation theory we refer to the extensive review by Onida, Reining and Rubio [8].

In this article we report calculations of the quasiparticle bandstructure of GaN and the II-VI compounds ZnO, ZnS and CdS in the zinc-blende structure. The *GW* method is defined as a perturbation to a system of non-interacting electrons, and we use density-functional theory (DFT) together with the Kohn-Sham concept of *fictitious* non-interacting particles as starting

point for our calculations. Unlike in Kohn-Sham DFT a self-consistent solution of the many-body perturbation would successively introduce higher order electron-electron interactions with every iteration step. These enter in the set of Hedin's equation for the Green's function [7] through the vertex function Γ, which up until now can only be solved fully for simple model systems. For this reason we refrain from any self-consistent treatment within the GW equations themselves[1] and remain with the zeroth order in the self-energy ($\Sigma_0 = iG_0W_0$), which typically gives bandstructures for weakly correlated quasiparticles in good agreement with valence-band photo-electron spectroscopy [9, 10]. In the G_0W_0 approximation to Σ the input Green's function and thus also the self-energy becomes dependent on the ground state calculation and hence the exchange-correlation functional used. This dependence is a central aspect of this article.

The Kohn-Sham eigenvalues of the commonly used local-density approximation (LDA) to the exchange-correlation potential give a particularly poor account of the electronic bandstructure in the II-VI materials and also to some extend in GaN. This is largely due to the inherent self-interaction effects in the LDA introduced by the cation semicore d-electrons [11, 12, 13]. The exact-exchange approach to density-functional theory (EXX) on the other hand is naturally self-interaction free. Contrary to the LDA and its gradient-corrected flavours (GGAs) the exchange potential in EXX-DFT only implicitly depends on the electron density via the Kohn-Sham orbitals, a point that we will further elucidate in later sections. Since the local exchange potential is constructed from the non-local Fock operator via the optimized effective potential method we prefer to abbreviate this approach by OEPx instead of EXX.

Due to its relationship with Hartree-Fock, OEPx has so far featured more prominently in atomic and molecular physics but recently applications to extended systems have also flourished [14, 15, 16, 17, 18, 19, 20, 21, 22, 23, 24, 25]. In these calculations a remarkably good agreement with experiment for the band gaps over a range of semiconductors has been reported. All DFT exact-exchange studies for group-III-nitrides and II-VI compounds [18, 19, 20, 21], however, have in common that the cation d-electrons have effectively been removed from the calculation by modelling their interaction with the valence electrons in terms of a pseudopotential. Although freezing the d-electrons in the core of a pseudopotential is computationally very efficient, it leads to a distinct disagreement between theory and experiment for the strucural properties as shown by several LDA studies [26, 27, 28]. In all calculations presented in this article the d-electrons were explicitly taken into account. Apart from improving the structural properties the inclusion of the d-electrons also has a profound effect on the electronic structure. We find that applying the OEPx approach leads to an improved description of the d-electron hybridisation compared to the LDA and therefore also to a better agreement between (I)PES data and our quasiparticle energy calculations.

If applied in an all-electron fashion, GW excited state calculations based on an LDA ground state will to a large extend remove the spurious self-interaction inherent to the LDA [29, 30, 31, 32]. When a pseudopotential concept is applied on the other hand the self-interaction of those core states that are locked away in the pseudopotential cannot be corrected by the GW approach. Thus, when semicore states that contribute to the chemical bonding or hybridise with valence states are present, all core states whose wavefunctions overlap strongly with these semicore states must be included explicitly as previous LDA based GW calculations demonstrate [33, 34, 35]. A key result of or our approach is that if exact-exchange pseudopotentials [36, 37] are used in the OEPx calculations it is sufficient to treat only the d-electrons as valence electrons. The s and p electrons of the same shell can be frozen in the core of the pseudopotential, because the self-interaction is already absent from the exact-exchange pseudopotentials and hence will not have to be removed by the GW calculation. The absence of self-interaction from

---

[1] We will briefly allude to some of the controversial issues pertaining to self-consistency in GW in later sections.

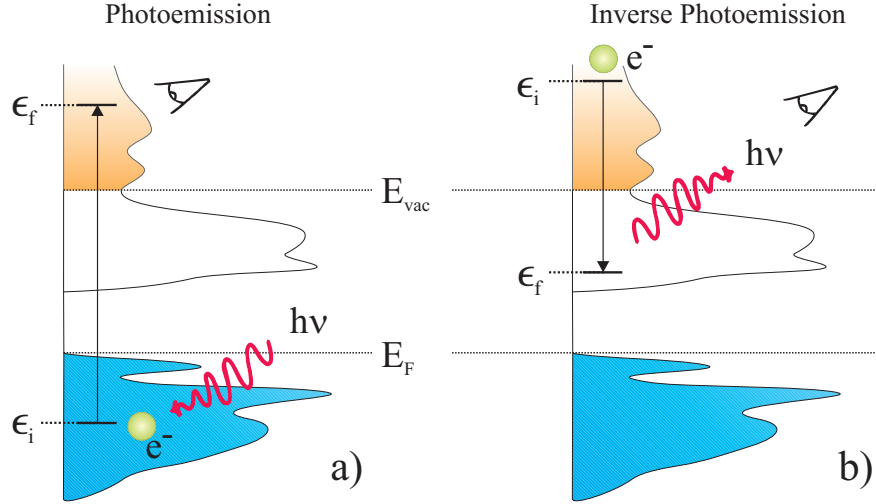Photoemission   Inverse Photoemission

Figure 1. Schematic of the photoemission (PES) and inverse photoemission (IPES) process. In PES (left) an electron is excited from an occupied valence state (lower shaded region) into the continuum (upper shaded region) starting above the vacuum level E_{vac} by an incoming photon. In IPES (right) an injected electron with kinetic energy $\epsilon_i = E_{kin}$ undergoes a radiative transition into an unoccupied state (white region) emitting a photon in the process.

the OEPx ground state gives rise to the aforementioned improvement in the description of the d-electron hybridisation compared to the LDA. This leads us to the hypothesis that the exact-exchange ground state constitutes the better starting point for subsequent GW calculations for this material class.

In fact up until now only two exact-exchange based quasiparticle energy calculations have been reported in the literature for GaN [20, 21]. In both cases, however, the d-electrons were treated as part of the frozen core. In this article we report for the first time exact-exchange calculations including the d-electrons. For II-VI compound our exact-exchange based GW studies are the first so far.

2. Probing the Electronic Structure by Photoemission

2.1. Photo-Electron Spectroscopy and the Quasiparticle Concept

In photo-electron spectroscopy (PES) electrons are ejected from a sample upon irradiation with visible or ultraviolett light (UPS) or with X-rays (XPS), as sketched in Fig. 1a. The energy of the bound electron states ϵ_i can be reconstructed from the photon energy $h\nu$ and the kinetic energy E_{kin} of the photoelectrons that reach the detector[2]

$$\epsilon_i = h\nu - E_{kin} \quad . \tag{2.1}$$

Equation (2.1) defines the binding energy of the electron in the solid.

By inverting the photoemission process, as schematically shown in Fig. 1b, the unoccupied states can be probed. An incident electron with energy E_{kin} is scattered in the sample emitting *bremsstrahlung*. Eventually it will undergo a radiative transition into a lower-lying

---

[2] Throughout this article the top of the valence bands is chosen as energy zero.

unoccupied state, emitting a photon that carries the transition energy $h\nu$. The energy of the final, unoccupied state can be deduced from the measured photon energy according to

$$\epsilon_f = E_{kin} - h\nu \quad . \tag{2.2}$$

This technique is commonly referred to as inverse photoemission spectroscopy (IPES) or bremsstrahlung isochromat spectroscopy (BIS).

The experimental observable in photoemission spectroscopy is the photocurrent. Since the energy dependence of the transition matrix elements is usually weak and smooth, structures in the photoemission spectrum can be associated with features in the density of states (DOS), i.e. the imaginary part of the one-particle Green function [3] [8, 38]

$$A(\mathbf{r}, \mathbf{r}'; \epsilon) = \frac{1}{\pi} \mathrm{Im}\, G(\mathbf{r}, \mathbf{r}'; \epsilon) = \sum_s \psi_s(\mathbf{r}) \psi_s^*(\mathbf{r}') \delta(\epsilon - \epsilon_s) \quad . \tag{2.3}$$

The sum in the last expression runs over all states s the system can assume and the photocurrent is then the surface weighted integral over the diagonal part of the spectral function $A(\mathbf{r}, \mathbf{r}'; \epsilon)$. We note, however, that with respect to the measured intensities a photoemission spectrum should be viewed as a noticeably distorted spectral function. In particular when selection rules become important certain peaks in the spectral function may be significantly reduced or may even disappear completely. The energies ϵ_s in equation (2.3) are the excitation energies of the many-body state created by the addition or removal of the photo-electron and $\psi_s(\mathbf{r})$ gives the transition amplitude from the N to the $N \pm 1$-body state. In many-body quantum mechanics ϵ_s and $\psi_s(\mathbf{r})$ are defined as [3, 6, 38, 39, 40, 41, 42]:

$$\left. \begin{array}{rcl} \epsilon_s & = & E(N+1, s) - E(N) \\ \psi_s(\mathbf{r}) & = & \langle N | \hat{\psi}(\mathbf{r}) | N+1, s \rangle \end{array} \right\} \quad \text{for} \quad \epsilon_s \geq E_F \tag{2.4}$$

$$\left. \begin{array}{rcl} \epsilon_s & = & E(N) - E(N-1, s) \\ \psi_s(\mathbf{r}) & = & \langle N-1, s | \hat{\psi}(\mathbf{r}) | N \rangle \end{array} \right\} \quad \text{for} \quad \epsilon_s < E_F \tag{2.5}$$

Here E_F is the Fermi energy of the system. The states $|N, s\rangle$ are many-body eigenstates of the N-electron Schrödinger equation $\hat{H}|N, s\rangle = E(N, s)|N, s\rangle$, $\hat{H}$ is the many-body Hamiltonian and $E(N, s) = \langle N, s | \hat{H} | N, s \rangle$ is the corresponding total energy. The field operator $\hat{\psi}(\mathbf{r})$ annihilates an electron from the many-body states $|N+1\rangle$ or $|N\rangle$. The representation given in equation (2.4) and (2.5) is particularly insightful because it allows a direct interpretation of ϵ_s as photo-excitation energy from the N-particle ground state with total energy $E(N)$ into an excited state s of the $(N$-1)-particle system with total energy $E(N-1, s)$ upon removal of an electron in the photoemission process. Similarly the addition energy that is released in the radiative transition in inverse photoemission is given by the total energy difference of the excited $(N+1)$-particle system and the ground state.

Via the field operator formalism the many-body Hamiltonian can be transformed into a single-particle Hamiltonian[4] [42]: $\hat{H}(\mathbf{r}, \mathbf{r}'; \epsilon) = \hat{h}_0(\mathbf{r}) + \Sigma(\mathbf{r}, \mathbf{r}'; \epsilon)$. All electron-electron interaction terms are rolled up in the non-local, energy dependent self-energy Σ and the remaining contributions are given by $\hat{h}_0(\mathbf{r}) = -\frac{1}{2}\nabla^2 + v_{ext}(\mathbf{r})$. The single particle Green's function

$$G(\mathbf{r}, \mathbf{r}'; \epsilon) = \langle \mathbf{r} | [\hat{H}(\epsilon) - \epsilon]^{-1} | \mathbf{r}' \rangle = \lim_{\eta \to 0^+} \sum_s \frac{\psi_s(\mathbf{r}) \psi_s^*(\mathbf{r}')}{\epsilon - (\epsilon_s + i\eta\, \mathrm{sgn}(E_f - \epsilon_s))} \tag{2.6}$$

---

[3] Atomic units $4\pi\epsilon_0 = h = e = m_e = 1$, where e and m_e are the charge and mass of an electron, respectively, will be used in the remainder of this article.

[4] Since the nuclei are assumed to be stationary throughout this article, the nucleus-nucleus interaction contributes only a constant to the total energy, whereas the electron-nucleus interaction can be represented by an external potential $v_{ext}(\mathbf{r})$.

then satisfies the Dyson equation

$$G^{-1}(\mathbf{r}, \mathbf{r}'; \epsilon) = \left[\epsilon - \hat{h}_0(\mathbf{r})\right] \delta(\mathbf{r} - \mathbf{r}') - \Sigma(\mathbf{r}, \mathbf{r}'; \epsilon) \tag{2.7}$$

and by inserting equation (2.6) into (2.7) one immediately finds that ϵ_s and $\psi_s(\mathbf{r})$ are solutions to

$$\hat{h}_0(\mathbf{r})\psi_s(\mathbf{r}) + \int d\mathbf{r}' \Sigma(\mathbf{r}, \mathbf{r}'; \epsilon_s)\psi_s(\mathbf{r}') = \epsilon_s \psi_s(\mathbf{r}) \quad . \tag{2.8}$$

The poles of the Green's function therefore correspond to the real electron addition and removal energies ϵ_s and form a branch-cut infinitesimally above (below) the real energy axis for occupied (unoccupied) states.

So far (2.4) to (2.8) have been exact, which is of limited use for practical computational schemes. To establish a link to photoemission spectroscopy of delocalised valence states it is helpful to introduce Landau's concept of *quasiparticles* [43]. This new entity can be considered as a combination of an electron or hole with its surrounding polarisation cloud or in other words as the collective response of the interacting many-body system upon photo-excitation. Switching to the quasiparticle picture is consistent with analytically continuing the self-energy to the complex energy domain. The quasiparticle poles (now at complex energy) each represent the effect of many of the infinitesimally closely spaced poles just above (below) the real axis. We will return to this point later in this section.

To motivate the association of *quasiparticles* with particle-like excitations we turn again to the spectral function. For non-interacting electrons the spectral function consists of a series of delta peaks

$$A_{sn}(\epsilon) = \langle \psi_s(\mathbf{r})|A(\mathbf{r}, \mathbf{r}'; \epsilon)|\psi_n(\mathbf{r}')\rangle = \delta_{sn}\delta(\epsilon - \epsilon_s), \tag{2.9}$$

each of which corresponds to the excitation of a particle. The many-body states $|N\rangle$ and $|N \pm 1\rangle$ are represented by a single Slater determinant and the excited state configurations by a single creation ($\hat{a}_s$) or anihilation ($\hat{a}_s^\dagger$) operator acting on the ground state: $|N + 1, s\rangle = \hat{a}_s^\dagger|N\rangle$. The excitation energies ϵ_s and the wavefunctions $\psi_s(\mathbf{r})$ are thus the eigenvalues and eigenfunctions of the single-particle Hamiltonian.

When the electron-electron interaction is turned on, the electrons can no longer be regarded as independent particles. As a consequence the matrix elements of the spectral function $A_{sn}(\epsilon)$ will contain contributions from many non-vanishing transition amplitudes. If these contributions merge into a clearly identifiable peak that appears to be derived from a single delta-peak broadened by the electron-electron interaction this structure can be interpreted as single-particle like excitation – the *quasiparticle*. The broadening of the quasiparticle peak in the spectral function is associated with the lifetime τ of the excitation due to electron-electron scattering, whereas the area underneath the peak is interpreted as the renormalisation Z of the quasiparticle. This renormalisation factor quantifies the reduction in spectral weight due to electron-electron exchange and correlation effects compared to an independent electron. In summary a quasiparticle peak in the spectral function will exhibit the following shape

$$A_s(\epsilon) \approx \frac{Z_s}{\epsilon - (\epsilon_s + i\Gamma)} \quad . \tag{2.10}$$

In contrast to the exact energies of the many-body states, which are poles of the Green's function on the real axis, the quasiparticle poles reside in the complex plane and are no longer eigenvalues of the single-particle Hamiltonian. The real part of this complex energy is associated with the energy of the quasiparticle excitation and the imaginary part with its inverse lifetime $\Gamma = 2/\tau$.

Apart from quasiparticle excitations a typical photoemission experiment provides a rich variety of additional information. In core-electron emission for instance inelastic losses or multi-electron excitations such as shake-ups and shake-offs lead to satellites in the spectrum. These are

genuine many-body effects that are not contained in the quasiparticle approximation. However, since we are primarily interested in the description of valence bands in semiconductors these many-body effects are not important for interpreting the spectral features. For a more indepth discussion of these many-body effects we therefore refer the interested reader to the following articles [38, 44, 45, 46, 47].

Before we introduce the GW approximation to the self-energy as a tractable computational approach for calculating the quasiparticle energies we will briefly address the reconstruction of bandstructure information from the measured photo-electron spectra. By varying the angle of incidence (angle resolved photo-electron spectroscopy (ARPES) [3] and $\mathbf{k}$-resolved inverse photo-electron spectroscopy (KRIPES) [6]) dispersion relations of the excitated states can be obtained. However, since the emitted photons or electrons inevitably have to pass the surface of the crystal to reach the detector, information about their transverse momentum $k_\perp$ is lost. This is due to the fact that the translational invariance is broken at the surface and only the parallel momentum component $k_\parallel$ is conserved.

In order to reconstruct the three-dimensional bandstructure of the solid assumptions are often made about the dispersion of the final states [1, 2, 4, 5, 48]. Alternatively *ab initio* calculations as described in this article can aid in the assignment of the measured peaks. Only recently absolute band mapping has been reported in secondary electron emission (SEE) experiments [49] and also for a technique combining ARPES with very low-energy electron diffraction (VLEED) [50].

State of the art spectroscopy techniques of course allow the variation of many more parameters than just the angle of incidence. A more in-depth discussion of photoemission experiments will, however, go beyond the scope of this article and we refer the reader to references [3] and [6] for more details.

2.2. The GW Formalism

To solve the Dyson equation (2.7) for real systems one typically applies Hedin's GW approximation [7] for the self-energy. Assuming that the quasiparticles interact only weakly via the screened Coulomb interaction W the self-energy in GW is then given as

$$\Sigma_{xc}^{GW}(\mathbf{r}, \mathbf{r}'; \epsilon) = \frac{i}{2\pi} \int_{-\infty}^{\infty} d\epsilon' e^{i\epsilon' \delta} G(\mathbf{r}, \mathbf{r}'; \epsilon + \epsilon') W(\mathbf{r}, \mathbf{r}'; \epsilon') \tag{2.11}$$

where δ is an infinitesimal, positive time. In practice one starts from a system of non-interacting particles with energies ϵ_i and wavefunctions $\phi_i(\mathbf{r})$. The non-interacting Green's function is defined analogous to equation (2.6) as[5]

$$G_0(\mathbf{r}, \mathbf{r}', \epsilon) = \lim_{\eta \to 0^+} \sum_i \frac{\phi_i(\mathbf{r}) \phi_i^*(\mathbf{r}')}{\epsilon - (\epsilon_i + i\eta \, \mathrm{sgn}(E_f - \epsilon_i))}. \tag{2.12}$$

The quantum state indices i and s are short for the composite of band index n and wave vector $\mathbf{k}$. In the random phase approximation (RPA) the dielectric function

$$\varepsilon(\mathbf{r}, \mathbf{r}', \epsilon) = \delta(\mathbf{r} - \mathbf{r}') - \int d\mathbf{r}'' v(\mathbf{r} - \mathbf{r}'') \chi_0(\mathbf{r}'', \mathbf{r}'; \epsilon) \tag{2.13}$$

is connected to the independent particle polarisability

$$\chi_0(\mathbf{r}, \mathbf{r}', \epsilon) = -\frac{i}{2\pi} \int_{-\infty}^{\infty} d\epsilon' G_0(\mathbf{r}, \mathbf{r}'; \epsilon' - \epsilon) G_0(\mathbf{r}', \mathbf{r}; \epsilon') \tag{2.14}$$

---

[5] Note that only spin unpolarised systems are considered here. All state summations therefore include the spin variable implicitly.

and the bare Coulomb interaction

$$v(\mathbf{r} - \mathbf{r}') = \frac{1}{|\mathbf{r} - \mathbf{r}'|} \tag{2.15}$$

is screened by the inverse dielectric function

$$W_0(\mathbf{r}, \mathbf{r}', \epsilon) = \int d\mathbf{r}'' \varepsilon^{-1}(\mathbf{r}, \mathbf{r}''; \epsilon) v(\mathbf{r}'' - \mathbf{r}') \quad . \tag{2.16}$$

For numerical convenience and physical insight we separate the GW self-energy (2.11) according to $\Sigma_{xc}^{GW} = \Sigma_x + \Sigma_c^{GW}$ with the two terms defined as

$$\Sigma_x(\mathbf{r}, \mathbf{r}') \quad = \frac{i}{2\pi} \int_{-\infty}^{\infty} d\epsilon' e^{i\epsilon'\delta} G(\mathbf{r}, \mathbf{r}'; \epsilon') v(\mathbf{r} - \mathbf{r}') \tag{2.17}$$

$$= -\sum_{i}^{occ} \phi_i(\mathbf{r}) v(\mathbf{r} - \mathbf{r}') \phi_i^*(\mathbf{r}')$$

$$\Sigma_c^{GW}(\mathbf{r}, \mathbf{r}'; \epsilon) = \frac{i}{2\pi} \int_{-\infty}^{\infty} d\epsilon' e^{i\epsilon'\delta} G(\mathbf{r}, \mathbf{r}'; \epsilon + \epsilon') \left[W(\mathbf{r}, \mathbf{r}'; \epsilon') - v(\mathbf{r} - \mathbf{r}') \right] \tag{2.18}$$

Σ_x is the Fock or bare exchange operator that we will revisit in section 2.5 and Σ_c^{GW} encompasses the dynamic correlation of the quasiparticles. Note that the definition of the self-energy in equation (2.7) implicitly includes the Hartree potential

$$v_H(\mathbf{r}) = \int d\mathbf{r}' \, n(\mathbf{r}') v(\mathbf{r} - \mathbf{r}') \tag{2.19}$$

with $n(\mathbf{r})$ being the electron density, whereas in this section the Hartree potential is separated from the GW self-energy. Inserting Σ_{xc} and the quasiparticle Green's function (2.6) into (2.7) the Dyson equation becomes

$$\left[\hat{h}_0(\mathbf{r}) + v_H(\mathbf{r}) \right] \psi_s(\mathbf{r}) + \int d\mathbf{r}' \Sigma_{xc}^{GW}(\mathbf{r}, \mathbf{r}'; \epsilon_s) \psi_s(\mathbf{r}') = \epsilon_s \psi_s(\mathbf{r}) \tag{2.20}$$

This equation, also referred to as *quasiparticle equation*, can then be solved for the quasiparticle energies and wavefunctions.

In principle the set of equations (2.11) to (2.16) could be solved self-consistently via the use of the Dyson equation (2.7) expressed now in terms of the non-interacting Greens function G_0 (and for brevity written in operator notation)

$$G = G_0 + G_0 \left[v_H + \Sigma_{xc}^{GW} \right] G \quad . \tag{2.21}$$

A crucial point to note, however, is that at each iteration higher order diagrams would have to be included, because the GW approximation is only equivalent to the first iteration of Hedin's equations [7], which are an exact set of equations for the Green's function and the self-energy. Both the polarisability $P = -iGG\Gamma$ and the self-energy $\Sigma = iG\Gamma W$ contain the vertex function Γ. Solving equations (2.11) to (2.21) *self-consistenly* is therefore *inconsistent* with Hedin's equations if no higher order electron-electron interactions are included via the vertex function Γ.

We can nevertheless group solutions to Hedin's GW equations (2.11) to (2.16) into three categories: self-consistent ($\Sigma = iGW$), partially self-consistent ($\Sigma = iGW_0$) and non self-consistent ($\Sigma = iG_0W_0$). Only GW_0 and GW fulfill certain sum rules including particle number conservation [51], which give rise to an improved description of ground state total energies [52, 53]. Spectral features, on the other hand, broaden with increasing number of iterations in the self-consistenty cycle, as was first observed for the homogeneous electron gas [52]. Similarly,

for closed shell atoms the good agreement with experiment for the ionisation potential in G_0W_0 is lost upon iterating the equations to self-consistency [54].

For bulk materials self-consistent GW calculations also exhibit a broadening of the spectral features compared to G_0W_0 [55, 56, 57, 58]. In pseudopotential GW calculations for bulk silicon this leads to a gross overestimation of the fundamental band gap [55], whereas an all-electron GW calculations yield band gaps in seemingly good agreement with experiment [58]. This discrepancy between pseudopotential and all-electron GW calculations has, to the best of our knowledge, not yet been resolved and is currently being discussed controversially in the literature (see for instance [32, 54, 59]).

Since addressing the issue of self-consistency in more detail would lead beyond the scope of this article we terminate the self-consistency cycle in our quasiparticle energy calculations after the first iteration, when the self-energy is given by $\Sigma_0^{GW} = iG_0W_0$ and solve the quasiparticle equation (2.20) for the excitation energies. This procedure implies, however, that the quasiparticle spectrum might now depend on the input Green's function, G_0, a crucial aspect that we will address in the following.

2.3. DFT and the Kohn-Sham Bandstructure

Density-functional theory (DFT) is probably the most widely used computational electronic structure method today for systems containing a large number of atoms. The central quantities in DFT are the electron density $n(\mathbf{r})$ and the total energy E_{tot}. The latter is a functional of the former and attains its minimum at the exact ground state density, as proven by Hohenberg and Kohn [60]. This formalism was turned into a tractable computational scheme by Kohn and Sham [61], by observing that the system of interacting particles can be mapped onto a fictious system of non-interacting particles that reproduce the same density as the many-body problem of interest.

Kohn and Sham divided the total energy into known contributions such as the kinetic energy of the non-interacting particles T_s, the Hartree energy

$$E_H[n] = \frac{1}{2} \int d\mathbf{r}\, n(\mathbf{r}) v_H(\mathbf{r}) \tag{2.22}$$

and the external energy

$$E_{ext}[n] = \int d\mathbf{r}\, n(\mathbf{r}) v_{ext}(\mathbf{r}) \quad . \tag{2.23}$$

and an unknown remainder. This last term includes all electron-electron interactions beyond the Hartree mean-field and is defined as the exchange-correlation energy

$$E_{xc}[n] = E_{tot}[n] - T_s[n] - E_{ext}[n] - E_H[n] \quad . \tag{2.24}$$

The electron density

$$n(\mathbf{r}) = \sum_i^{occ} |\phi_i(\mathbf{r})|^2 \tag{2.25}$$

is composed of the occupied Kohn-Sham orbitals $\phi_i(\mathbf{r})$ that are solutions of the Kohn-Sham equation

$$\left[-\frac{\nabla^2}{2} + v_{ext}(\mathbf{r}) + v_H(\mathbf{r}) + v_{xc}(\mathbf{r}) \right] \phi_i(\mathbf{r}) = \epsilon_i \phi_i(\mathbf{r}) \quad . \tag{2.26}$$

The exchange-correlation potential $v_{xc}(\mathbf{r})$ is formally defined as the functional derivative of the exchange-correlation energy

$$v_{xc}(\mathbf{r}) = \frac{\delta E_{xc}[n]}{\delta n(\mathbf{r})} \quad . \tag{2.27}$$

Equations (2.22) to (2.26) have to be solved self-consistently until convergence in the total energy is reached.

Since the exact form of the exchange-correlation functional is unknown[6] suitable approximations have to be found in practice. In this article we work in the local-density approximation (LDA) [61] or in the exact-exchange approximation to the optimised effective potential. Since the latter constitutes an important aspect of our work we will describe it in more detail in the following sections.

Contrary to the poles of the Green's function (2.4) the Kohn-Sham eigenvalues are Lagrange multipliers and are therefore primarily mathematical constructs. Strictly spoken only the highest occupied Kohn-Sham eigenvalue of exact DFT can be rigorously assigned to the ionisation potential [63, 64, 65]. For an extended system with well defined chemical potential this is equivalent to stating that the chemical potential in DFT is the same as the true one (Janak's theorem [66]). Furthermore Janak's theorem implies that for delocalised states the Kohn-Sham eigenvalues are close to ϵ_i and ϵ_f as defined in equation (2.1) and (2.2). Recently further justification for the interpretation of exact Kohn-Sham orbital energies as approximate vertical ionization potentials was given for finite systems [67]. For atoms and small molecules, where accurate *ab initio* densities were available, the Kohn-Sham eigenvalues were found to be very close to experimentally measured ionisation and excitation energies [67, 68]. Although, noteable deviations were observed if an LDA or GGA functional was employed instead, the Kohn-Sham eigenvalues still provide a good starting point for self-energy calculations in the framework of many-body perturbation theory.

Furthermore the true v_{xc} is a discontinuous function of the particle number N, which essentially implies that the value of v_{xc} jumps by a constant for finite $\mathbf{r}$ when the particle number is infinitesimally increased from $N - \delta$ to $N + \delta$. This discontinuity has a profound effect on the calculated band gaps of semiconductors and insulators [69, 70]. In the LDA or GGA the exchange-correlation potential is a smoothly varying function with respect to changes in the particle number, whereas the exchange potential in the exact-exchange formalism exhibits an integer discontinuity [71], but not necessarily of the correct size. We will further allude to this point in the following sections.

2.4. Connection between DFT and GW

Before we introduce the exact-exchange approximation to E_{xc} it is elucidating to draw a connection between many-body perturbation theory as described in section 2.1 and 2.2 and density-functional theory. In the original proof [70, 72] Sham and Schlüter made use of the fact that the Kohn-Sham density reproduces the exact electron density (Hohenberg-Kohn theorem [60]). Both the density of the interacting as well as the density of the non-interacting system can be obtained from the respective Green's function: $n(\mathbf{r}) = \frac{1}{\pi}\mathrm{Im}\int d\epsilon G(\mathbf{r}, \mathbf{r}; \epsilon)$, which leads to the *density condition*

$$0 = n(\mathbf{r}) - n_{\mathrm{KS}}(\mathbf{r}) = \frac{1}{2\pi}\mathrm{Im}\int d\epsilon \left[G(\mathbf{r}, \mathbf{r}; \epsilon) - G_{\mathrm{KS}}(\mathbf{r}, \mathbf{r}; \epsilon)\right]. \tag{2.28}$$

The Kohn-Sham Green's function, G_{KS}, entering this equation is an independent particle Green's function (2.12) constructed from the Kohn-Sham orbitals. Applying the Dyson equation (2.7)

---

[6] To be more precise the exact dependence of v_{xc} on the density alone is unknow. In the context of many-body perturbation theory the exact exchange-correlation potential can be expressed in terms of the Green's function and the self-energy via the Sham-Schlüter equation, introduced in the next section. Alternatively an exact representation of v_{xc} can be obtained in Görling-Levy perturbation theory [62].

transforms the density condition into the Sham-Schlüter equation

$$\int d\epsilon \int d\mathbf{r}' \int d\mathbf{r}'' G_{\mathrm{KS}}(\mathbf{r}, \mathbf{r}'; \epsilon)\tilde{\Sigma}_{xc}(\mathbf{r}', \mathbf{r}''; \epsilon)G(\mathbf{r}'', \mathbf{r}; \epsilon) = 0 \qquad (2.29)$$

where the self-energy that connects the interacting with the non-interacting system has been defined as

$$\tilde{\Sigma}_{xc}(\mathbf{r}, \mathbf{r}'; \epsilon) = \Sigma_{xc}(\mathbf{r}, \mathbf{r}'; \epsilon) - v_{xc}(\mathbf{r})\delta(\mathbf{r} - \mathbf{r}'). \qquad (2.30)$$

The exchange-correlation potential of density-functional theory can therefore be interpreted as the variationally best local approximation to the non-local, dynamic self-energy [73]. With regards to the interpretation of the Kohn-Sham eigenvalues as photoemission excitation energies, however, the Sham-Schlüter equation corroborates the conjecture that one has to go beyond the locality in time or space to improve on the density-functional treatment, even if the exact v_{xc} was known [73].

2.5. The Optimised Effective Potential Method and Exact-Exchange

In this section we will introduce the exact-exchange (EXX) approximation to density-functional theory. Following Kohn and Sham's idea of dividing the total energy into known and unknown contributions the exact-exchange energy E_x

$$E_x = -\frac{1}{2}\sum_{ij}^{occ} \int d\mathbf{r} \int d\mathbf{r}' \phi_i^*(\mathbf{r})\phi_j(\mathbf{r})v(\mathbf{r} - \mathbf{r}')\phi_j^*(\mathbf{r}')\phi_i(\mathbf{r}') \qquad (2.31)$$

can be isolated from E_{xc} leaving only the correlation part E_c to be approximated. In the exact-exchange only approach this correlation term is ignored[7] so that the total energy becomes

$$E_{tot}^{\mathrm{EXX}} = T_s[n] + E_{ext} + E_H + E_x \quad . \qquad (2.32)$$

In order to connect to the previous section we will take a different route than in most texts to derive the Kohn-Sham exchange-potential from this energy expression. We will show that the Sham-Schlüter equation naturally reverts to the *optimised effective potential* method (OPM) for the exchange-correlation potential [73, 74, 75, 76]. We therefore chose to denote the optimised effective potential in the exact-exchange approach by OEPx instead of EXX.

To derive the optimised effective potential (OEP) equations the Sham-Schlüter equation (2.29) is first linearised [77, 78, 73] by replacing the fully interacting Green's function, G, with the Kohn-Sham Green's function, G_{KS}. Further replacing the self-energy with only the exchange part (2.17), which is is equivalent to the Fock operator, and rearranging the resulting equation into the conventional form of a non-linear integral equation yields the equation for the OEPx potential [70, 74, 76, 79, 80]

$$\int d\mathbf{r}' \chi_0(\mathbf{r}, \mathbf{r}')v_x(\mathbf{r}') = \Lambda_{\mathrm{OEPx}}(\mathbf{r}) \qquad (2.33)$$

with

$$\Lambda_{\mathrm{OEPx}}(\mathbf{r}) = \int d\epsilon \int d\mathbf{r}' \int d\mathbf{r}'' G_{\mathrm{KS}}(\mathbf{r}, \mathbf{r}'; \epsilon)\Sigma_x(\mathbf{r}', \mathbf{r}'')G_{\mathrm{KS}}(\mathbf{r}'', \mathbf{r}; \epsilon). \qquad (2.34)$$

$\chi_0(\mathbf{r}, \mathbf{r}')$ is the independent particle polarisability, $\chi_0(\mathbf{r}, \mathbf{r}'; \epsilon = 0)$, as previously defined in the context of the GW approximation (equation (2.13)).

The exchange-potential v_x can be thought of as the best local potential approximating the non-local Fock operator [73]. It is important to emphasise, however, that by construction the

---

[7] Later in this section we will reintroduce the correlation energy in an approximate form that is commonly used in connection with exact-exchange DFT calculations.

total energy in Hartree-Fock is always smaller (or at most equal) and thus better than in the OEPx formalism [81], because the energy minimisation in the optimised effective potential method is subject to the constraint of the wavefunctions being solutions to the Kohn-Sham equation (2.26). The eigenvalues of the OEPx formalism, on the other hand, derive from an effective mean-field approach for non-interacting particles, whereas in Hartree-Fock they correspond to the energies of electrons interacting via Pauli but not Coulomb correlation. The Kohn-Sham particles in the valence and conduction bands are therefore governed by the same effective potential, which exhibits the correct asymptotic behaviour ($1/r$ decay for large distances in finite systems) in the OEPx.

In Hartree-Fock on the other hand virtual conduction electrons are only poorly accounted for and experience a different potential than the valence electrons. Since the Fock-operator contains the self-interaction correction only for the valence electrons, a virtual conduction electron interacts with all N valence electrons, in contrast to a valence electron, which interacts only with the remaining N-1 electrons. Thus, for a charge neutral system each valence electron in Hartree-Fock experiences a density of netcharge $+1$ and the correct $1/r$ potential decay results for finite systems. This stands in obvious contrast to the description of the virtual conduction electrons, that see a neutral charge density. Since excitations in the valence and conduction bands of solids leave the charge density largely unchanged the different treatment of valence and conduction electrons within Hartree-Fock appears to be unjustified. Indeed, as we will present in the following sections the OEPx eigenvalues are closer to the photo-electron excitation energies for the four semiconductors discussed in this article than the Hartree-Fock energies.

The exact-exchange potential v_x is only implicitly a function of the electron density via the Kohn-Sham orbitals. This is in accordance with the Hohenberg-Kohn theorem as can easily be seen by performing the functional derivative of the exact-exchange energy (2.31) with respect to the density. Applying first order perturbation theory yields the more familiar expression for the OEPx equation[8]

$$v_x(\mathbf{r}) = -\sum_i^{occ} \int d\mathbf{r}' \int d\mathbf{r}'' \left[\phi_i^*(\mathbf{r}') G_i(\mathbf{r}',\mathbf{r}'') \frac{\delta E_x}{\delta \phi_i^*(\mathbf{r}'')} + c.c. \right] \chi_0^{-1}(\mathbf{r}'',\mathbf{r}') \qquad (2.35)$$

with

$$G_i(\mathbf{r}',\mathbf{r}'') = \sum_{j\neq i} \frac{\phi_j(\mathbf{r})\phi_j^*(\mathbf{r}')}{\epsilon_j - \epsilon_i} \qquad . \qquad (2.36)$$

In OEPx calculations *local* correlation is frequently added by including the LDA correlation energy

$$E_c^{\text{LDA}}[n] = \int d\mathbf{r}\, \epsilon_c^{\text{HEG}}(n(\mathbf{r})) \qquad (2.37)$$

in the expression of the total energy (2.32). Here we follow the parametrization of Perdew and Zunger [82] for the correlation energy density $\epsilon_c^{\text{HEG}}(n(\mathbf{r}))$ of the homogeneous electron gas (HEG) based on the data of Ceperley and Alder [83].

Adding LDA correlation improves the ionisation potential of the constituent atoms as will be shown later, but has little affect on the quasiparticle bandstructures of the compound semiconductors presented in section 3.3.3. In the following we will refer to the OEP exact-exchange only scheme by OEPx in order to distinguish it from the scheme with added LDA correlation, termed OEPx(cLDA).

---

[8] Likewise this equation can be obtained from (2.33) by integrating out the frequency dependence of the inhomogeneity Λ_{OEPx}, which can be done analytically because Σ_x is a static operator.

The improvement of the exact-exchange approximation over the conventional LDA or GGA approach is largely due to the removal of the self-interaction in the OEPx formalism. Or in other words, the interaction of an electron with itself, as introduced by the Hartee potential (2.19), is fully removed by the exact v_x. Since the OEPx exchange potential derives from an orbital dependent functional it exhibits an integer discontinuity with respect to variations in the particle number [71] (as does the full OEP potential [65]), unlike the smoothly varying exchange-correlation potentials in LDA or GGA. For solids, however, it is still unclear how to interpret this discontinuity in OEPx bandstructure calculations [24]. This shall be of no immediate concern for our work because using the OEPx eigenvalues as input for the Green's function is formally well defined.

On a more important note we like to emphasise that the exact-exchange potential can be derived from the framework of many-body perturbation theory unlike v_{xc} in the LDA or GGA, for which this is only true in the jellium limit. Equation (2.33) therefore provides a rigorous connection between the exact-exchange Kohn-Sham system and GW. From this observation we draw the hypothesis that the OEPx approach provides a better starting point for quasiparticle energy calculations than LDA or GGA. In the remainder of this paper we will verify this hypothesis numerically for the four materials considered here.

As a side note we like to mention that part of the quasiparticle screening can already be incorporated on the level of DFT. Rooted in the generalised Kohn-Sham scheme [84], the so called screened-exchange approximation (sX-LDA) [84, 85, 86, 87] utilises an *ad hoc* model (typically Thomas-Fermi) to screen the exchange-interaction. Conceptionally the sX-LDA approach is similar to the screened-exchange (SEX) approximation in the framework of the GW method [88]. Bandstructures in the sX-LDA scheme are reported to be in good agreement with experiment for semiconductors and insulators [84, 85, 87]. This indicates that sX-LDA could be a viable alternative to the OEPx as a starting point for GW calculations. A numerical verification of this conjecture, however, will be left to future studies.

3. Shallow Semicore d-Electron Systems

The II-VI compounds and most of the group-III-nitrides are characterised by the semicore d-electrons introduced by the cation. Compared to other materials with semicore states the cation d-electrons in ZnO, ZnS and CdS have a small binding energy of around 9 eV [89, 90] and are thus energetically close to the valence states with mostly anion p-character. For GaN X-ray photoemission experiments report two peaks at 17.7 eV and 14.2 eV that have been attributed to the Ga $3d$ states and the N $2s$ bands, respectively [91] (see section 3.3.2 for bandstructure plots). In the Zn and Cd based semiconductors the p-d hybridisation is therefore larger than in GaN, which in turn exhibits stronger s-d coupling. The effect of this qualitative difference on the electronic wavefunctions and densities will be discuss in section 3.3.1.

In light of this argument it is essential to find a good description of the p-d and s-d coupling in order to calculate the structural and the electronic properties of these materials. In the past a common approximation has been to simply remove the d-electrons from the calculation and to model the interaction of the valence electrons with the atomic core by a pseudopotential (see next section). Although this is computationally very efficient it leads to a distinct disagreement between theory and experiment for the strucural properties [26, 27, 28] as well as for electronic excitations [33, 34, 35].

In the following section we will introduce the pseudopotential approximation and elucidate how shallow semicore electron systems can be treated consistently in our OEPx(cLDA)+GW approach for the electronic structure.

3.1. Core-Valence Partitioning and Pseudopotentials

The *pseudopotential* approach to electronic structure methods for polyatomic systems employs the more general concept of *core-valence partitioning*. Motivated by the observation that deep core states are relatively inert and do not contribute to chemical bonding they are often treated on a different footing than valence or semicore[9] electrons.

In *ab initio* pseudopotential calculations the potential due to the nuclei and the core electrons is replaced by an *ionic pseudopotential*. A good pseudopotential should be smooth and should describe the interaction with the remaining valence electrons of the atom well, while at the same time being transferable across chemically different environments. The pseudopotential is constructed by replacing the valence wavefunctions of the isolated atom by smooth, nodeless pseudowavefunctions inside a given cutoff radius. Inversion of the atomic Schrödinger equation then yields the atomic pseudopotential and by substracting out the Hartree and exchange-correlation potential generated by the pseudovalence states the ionic pseudopotential is obtained. For reciprocal-space electronic structure methods a substantial reduction of the computational cost can be gained in this way, because the oscillations of the atomic wavefunctions near the nucleus no longer have to be resolved by plane-waves. Once the pseudopotential has been generated the core electrons have been removed from the calculation of the polyatomic system and remain frozen inside the nucleus. Core relaxation and polarisation effects can thus not be taken into account, because the pseudopotential is typically not adjusted to the new chemical environment during the self-consistency cycle.

Since any calculation following core-valence partitioning can never be better than the accuracy with which the interactions between core and valence electrons have been treated [92], it has long been recognised that consistency is paramount. For DFT calculations with local or semi-local exchange-correlation functionals this is achieved by employing the same functional in the generation of the pseudopotential and the calculation of the extended or molecular system. In fact *ab initio* LDA or GGA pseudopotentials are now routinely applied in LDA or GGA calculations to a wide range of systems. When going beyond DFT, however, consistency will almost inevitably be violated. In quantum Monte Carlo calculations for example Hartree-Fock pseudopotentials are frequently employed [93], whereas *GW* calculations are almost exclusively based on an LDA or GGA ground state [10] and the respective pseudopotential [9]. One way of compensating for the lack of many-body pseudopotentials would be to introduce core polarisation effects into the pseudopotential [93, 94]. By extending the *GW* formalism to include core contributions in the dielectric screening and the self-energy such core-polarisation-potentials (CPP) have also been incorporated successfully into the *GW* method [95].

Ultimate consistency would of course imply to abolish pseudopotential-core-valence partitioning and to treat all electrons on the same footing. While DFT-all-electron methods have become a standard technique in condensed matter physics all-electron *GW* implementations are only slowly emerging. Early calculations were carried out in the atomic sphere approximation (ASA) to the linearised muffin-tin-orbital (LMTO) method [96, 97, 98, 99]. Only fairly recently *GW* calculations in the full-potential (FP-LMTO) [29, 32] or the full-potential linearised augmented-plane-wave (LAPW) method [30, 31, 58] have been reported, whereas the projector-augmented-wave (PAW) scheme [100, 101] falls into a mixed category. While the effect of the core-electrons on the valence electrons is included in the PAW method, the augmentation projectors are not updated in the calculation. That puts the treatment of the core electrons in PAW on the same footing as in a pseudopotential approach.

In order to reduce the size of the frozen core in the pseudopotential approach and therefore

---

[9] In the destinction between valence and core states, *semicore* states have binding energies between those of core and valence electrons, but hybridize with valence states or contribute to chemical bonding.

to move towards an all-electron description, more core electrons can be explicitly considered as valence electrons in the calculation [33, 34, 35, 59, 102]. Special care has to be taken, however, if an angular momentum channel has more than one bound state. The computational costs for treating core states in this fashion are moderate when localised basis sets are used [33, 34], but fromidable in a plane-wave implementation [35, 59, 102].
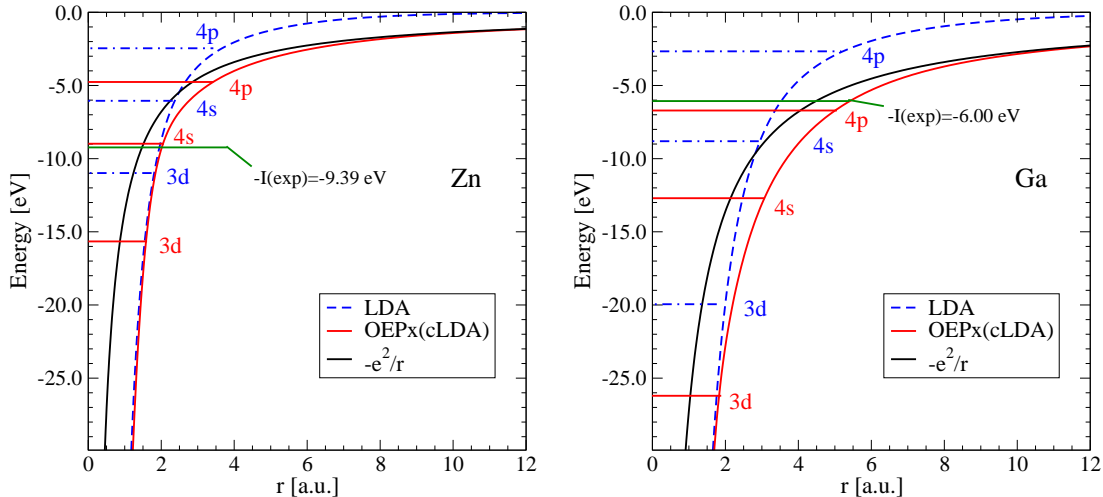

Figure 2. Effective Kohn-Sham potential for the neutral Zn (left panel) and Ga (right panel) atom: the OEPx(cLDA) potential (red line) reproduces the correct asymptotic decay $-e^2/r$ (black line), whereas the LDA (blue, dashed line) decays exponentially and thus underbinds the electrons. The atomic levels (shown as horizontal lines) are lowered in the OEPx(cLDA) approach compared to the LDA resulting in good agreement with the experimentally measured ionisation potential (green horizontal line).

Since the quality of the basis set in real and reciprocal space methods can be systematically monitored and increased simply by including more points or plane-waves we prefer to stay within the framework of plane-wave and so called *mixed-space* electronic structure calculations [103, 104] in this study. In order to capitalise on the "cost-effectiveness" of the pseudopotential approach and the numerical convenience of plane-waves we combine the *GW* excited state calculations with DFT ground state calculations in the exact-exchange formalism (denoted OEPx+*GW* in order to draw a distinction to *GW* calculations based on the LDA ground state, LDA+*GW*, which we perform for comparison). Employing exact-exchange pseudopotentials [36, 37] allows us to freeze the *s* and *p* electrons of the semicore *d*-shell in the core of the pseudopotential while retaining the *d*-electrons as valence states in the calculation (see also Tab. 1). Our numerical results for the quasiparticle bandstructures in the OEPx+*GW* formalism (sections 3.3.2, 3.3.3 and 3.3.4) show good agreement with available photo-electron spectroscopy data, which indicates that the dominant interaction between the core and valence electrons is exchange mediated and is well described by the exact-exchange pseudopotentials for the compounds considered here. This is one of the key results of our work and we will elucidate it further in later sections.

Figure 2 illustrates the improvement for the Kohn-Sham eigen-energies obtained in the OEPx(cLDA) formalism compared to the conventional LDA treatment for the Zn (on the left) and the Ga atom (on the right). In our work we follow the approach of Mourkara *et al.* [36] in

Table 1. Pseudopotential reference parameters: The electron configuration is given in the 2nd column with the core electron configuration in square brackets. The same core radius r_c (given in bohr) was used for all angular momentum components and the local component l_{loc} is listed in the 4th column. For N only s and p components are considered [105].

Cation	Configuration	r_c	l_{loc}	Anion	Configuration	r_c	l_{loc}
Zn	$[Ar]3d^{10}4s^2$	2.2	s	N	$[He]2s^22p^3$	1.5	p
Ga	$[Ar]3d^{10}4s^24p^1$	2.2	s	O	$[He]2s^22p^4$	1.6	d
Cd	$[Kr]4d^{10}5s^2$	2.2	s	S	$[Ne]3s^23p^4$	1.7	d

constructing the OEPx and OEPx(cLDA) pseudopotentials. The parameters for the LDA and exact-exchange pseudopotentials are taken to be the same and are listen in Table 1. Returning to Fig. 2 we observe that the effective Kohn-Sham potential (red line) follows the correct asymptotic $-e^2/r$ potential outside the atom (black line), whereas the the LDA potential (blue, dashed line) decays exponentially fast. The strong underbinding of the electrons inherent to the LDA is greatly reduced in the OEPx(cLDA) approach. This is largely due to the removal of the self-interaction in the OEPx(cLDA), which leads to a lowering of the atomic levels. Good agreement between the highest occupied electronic level and the experimental ionisation potential is then observed.

We will close this section with a brief overview of the compuational cost associated with our approach. For this purpose we will focus on the example of zinc-blende GaN. To converge the LDA full-shell pseudopotential ground state calculation, where the Ga $3s$ and $3p$ are treated as valence electrons, a plane wave cutoff of 300 Ry is needed. To achieve convergence of better than 0.1 eV in the quasiparticle energies a cutoff of 144 Ry for the correlation and 270 Ry for the exchange part of the GW self-energy is required [106][10]. For the computationally more intensive correlation part this is twice as much as is needed when the Ga $3s$ and $3p$ electrons are frozen in the core of the pseudopotential (see Tab. 2). Since the GW space-time method scales quadratically with the number of real-space points and cubically with the number of **G**-vectors doubling the cutoff increases the computational load by a factor that lies somewhere between 8 and 22 depending on how much the inversion of the dielectric function dominates the scaling. It is therefore desirable to keep the cutoff in plane wave GW calculations as low as possible.

A GW plane wave cutoff of 70 Ry for GaN can still be considered as moderate both in terms of memory and hard disk space usage as well as computational time. The OEPx+GW calculations for the zinc-blende structures presented here can still be carried out on a modern PC or workstation, whereas the memory and disk space requirements for the full-shell GW calculations quickly reach dimensions presently only available on high-performance computing clusters and at super computer facilities.

The computationally most intensive part of our OEPx+GW approach are currently the exact-exchange calculations. Since we follow the OEP scheme for solids developed by Görling [17] an explicit calculation and inversion of the static polarisability is also required for the OEPx ground state calculations (see equation (2.35)). In our experience every iteration of the OEPx self-consistency cycle in this implementation is comparable to a full GW calculation in terms of hardware requirements and run time. Altogether between 5 and 8 OEP cycles are needed to converge the exact-exchange calculations presented in this article. Recently, however, a new OEP scheme has been proposed [107, 108, 109], which circumvents an explicit

[10] This compares well to parameters for other materials [59, 102], although the parameters in Ref. [35] appear to be somewhat low.

Table 2. Computational parameters: zinc-blende lattice constant (a_{ZB}) in Å, plane-wave cutoff (E_{cut}), reduced cutoff for the inversion of χ_0 in OEPx (χ_{cut}) and the band cutoff for the Green function (b_{cut}) are listed in Rydberg. Column 5 gives the change in the macroscopic dielectric constant (ε_M) in percent when the non-local (NL) component of the OEPx(cLDA) pseudopotential is included and the last column the resulting change in the quasiparticle band gap.

	a_{ZB}	E_{cut}	χ_{cut}	b_{cut}	$\Delta\varepsilon_M/\varepsilon_M$	$E_{gap}^{NL} - E_{gap}$
GaN	4.500	70 Ry	45 Ry	40 Ry	-10 %	0.07 eV
ZnO	4.620	60 Ry	35 Ry	56 Ry	-15 %	0.15 eV
ZnS	5.400	60 Ry	35 Ry	40 Ry	0 %	0.00 eV
CdS	5.818	50 Ry	30 Ry	24 Ry	+8 %	-0.03 eV

solution of equation (2.35). This alternative scheme promises to be computationally much more efficient than our current implementation and therefore to substantially reduce the cost of the OEPx+*GW* approach.

3.2. Computational Details

All ground state calculations are performed with the pseudopotential plane-wave DFT code `SFHIngX` [110]. The OEPx formalism for solids [17] has recently been added [25] to this program package. For the DFT calculations in the local-density approximation [61] we use the parameterisation by Perdew and Zunger [82] of the Ceperley and Alder data for the homogenous electron gas [83].

All LDA pseudopotentials are constructed with the `fhi98PP` generator [111], in the Troullier-Martins (TM) scheme [112] and transformed to the non-local, separable Kleinman-Bylander form [113]. For the four compounds presented in this article our LDA calculations with these pseudopotentials reproduce the bandstructure of all-electron LDA calculations in the (linearised) augmented-plane-wave plus local orbital ((L)APW+lo) approach [114] to within 0.1 eV [115]. For the OEPx and OEPx(cLDA) pseudopotentials we follow the method developed by Moukara *et al.* [36].

The *GW* calculations are performed employing the *GW* space-time approach [103] in the `gwst` implementation [104, 116]. To accelerate the convergence with respect to the number of k-points and to avoid numerical instabilities arising from the Coulomb singularity at $\mathbf{k} = 0$ in reciprocal space we treat head and wings of the dielectric matrix (2.13) in kp-perturbation theory [88, 117, 104]. In this approach the inverse of the head of the inverse dielectric matrix is then equivalent to the macrosopic dielectric constant ε_M in the RPA. We find that ε_M is fully converged if a $4\times4\times4$ **k**-grid with an offset of $[\frac{1}{2}, \frac{1}{2}, \frac{1}{2}]$ is used for the Brillouin zone integration. A $4\times4\times4$ **k**-grid with no offset then proves to be sufficient for the full *GW* calculation. The non-local part of the OEPx(cLDA) pseudopotentials, which is fully taken into account in our implementation, reduces the RPA macroscopic dielectric constant ε_M in GaN and ZnO, but increases it in CdS, as can be seen in Tab. 2. The quasiparticle band gap, however, is modified only slightly. More details will be given elsewhere [118].

With respect to the plane-wave cutoff (E_{cut}) in all DFT and *GW* calculations the single particle energies are converged to better than a tenth of an eV for the values listed in Tab. 2. The static polarisability in the OEP calculations is set up and inverted in a smaller plane-wave basis with a reduced cutoff energy χ_{cut}. Further increasing χ_{cut} changes the eigenvalues by less than 0.01 eV [25]. Finally all unoccupied bands with energy $\epsilon - E_F < b_{cut}$ are included in the *GW* Green's function. All calculations are carried out for zinc-blende structures. In order

to facilitate an unambigious comparison with experiment or in other words to benchmark the performance of our computational approach against the exact theory all calculation are carried out at the experimental lattice constants, as reported in column 1 of Tab. 2.

To solve the quasiparticle equation (2.20) we approximate the quasiparticle wavefunctions by the Kohn-Sham eigenfunctions: $\psi_{n\mathbf{k}}(\mathbf{r}) = \phi_{n\mathbf{k}}(\mathbf{r})$. For the upper valence and conduction bands of standard semiconductors numerical investigations indicate that this approximation is well justified [9, 10], but it breaks down for certain surface [119, 120, 121, 122] and cluster states [123, 124]. We will leave an analysis of the quasiparticle wavefunctions to future studies and instead solve the diagonal quasiparticle equation

$$\epsilon_{n\mathbf{k}}^{qp} = \epsilon_{n\mathbf{k}}^{\mathrm{DFT}} + \langle \phi_{n\mathbf{k}} | \Sigma_{xc}^{GW}(\epsilon_{n\mathbf{k}}^{qp}) - v_{xc} - \Delta\mu | \phi_{n\mathbf{k}} \rangle \tag{3.1}$$

iteratively for the quasiparticle energies $\epsilon_{n\mathbf{k}}^{qp}$. At every iteration step the DFT energies are shifted by a constant $\Delta\mu$ that aligns the Fermi energies before and after applying the GW self-energy corrections. This makes the solution of the quasiparticle equation robust against different energy zeros of the exchange-correlation potential, in particular if the energy zero is not the same as that of the self-energy. The alignment constant $\Delta\mu$ was first introduced by Hedin [7] for the electron gas to simulate to some extent the effects of self-consistency in G. Later it was shown for a model system [125] that $\Delta\mu$ is instrumental in keeping violations of charge conservation negligible.

3.3. Electronic Structure of II-VI Compounds and Group-III-Nitrides

3.3.1. Electron Density and Wavefunctions Approximating the quasiparticle wavefunctions with the Kohn-Sham eigenfunctions introduces a dependence on the exchange-correlation functional into the GW calculation. Changing the functional from LDA to OEPx(cLDA) in the ground state calculation will modify the wavefunctions and subsequently alter the interaction of the quasiparticles. To elucidate these changes we have plotted the charge densities and charge density difference for ZnS and GaN along the [111] direction through the unit cell (middle panel on the right of Fig. 3 and 4, respectively). In the panel on the left hand side the differences are broken down in terms of the partial charge densities $\Delta n_i(\mathbf{r})$ that have been obtained by summing over all wavefunctions in the bands indicated. In Ga the 3d electrons are lower in energy than in Zn (see Fig. 2). The d-band complex is therefore found closer to the N 2s states in GaN than to the S 3s in ZnS, as the bandstructures in Fig. 6 and 8 illustrate. For ZnS we can thus clearly distinguish between the partial density of bands with mostly S 3s (dashed green line), Zn 3d (red line) and sp character (blue line), whereas for GaN we included the N 2s states in the sum over the d-bands (red line). To visualise the spatial variation of the partial electron density difference we included cross-section plots for the sp-valence states (top panel) and d-states (lower panel) of ZnS in Fig. 3.

Inspection of Fig. 3 and 4 shows that the electron densities in LDA and OEPx(cLDA) are nearly identical and almost indistinguishable on the scale of the plot. A magnification of the density difference, however, reveals small charge accumulations in the bonding region and on the cation for the OEPx(cLDA) ground state compared to the LDA one. Comparing GaN with ZnS the charge localisation on the Ga atoms in the OEPx(cLDA) approach is found to be more pronounced than on the Zn atoms. A closer look at the partial densities elucidates that this qualitative difference arises from the different d-electron hybridisation in these two compounds. In ZnS the d-states hybridise with the sp-valence states so that the removal of self-interaction in the OEPx(cLDA) leads to a stronger localisation of the d-electrons (red line) on the Zn atom, whereas the valence electrons (blue line) are drawn from Zn into the bonding region. The two effects are of opposite nature and as a result a negligible overall charge density difference is
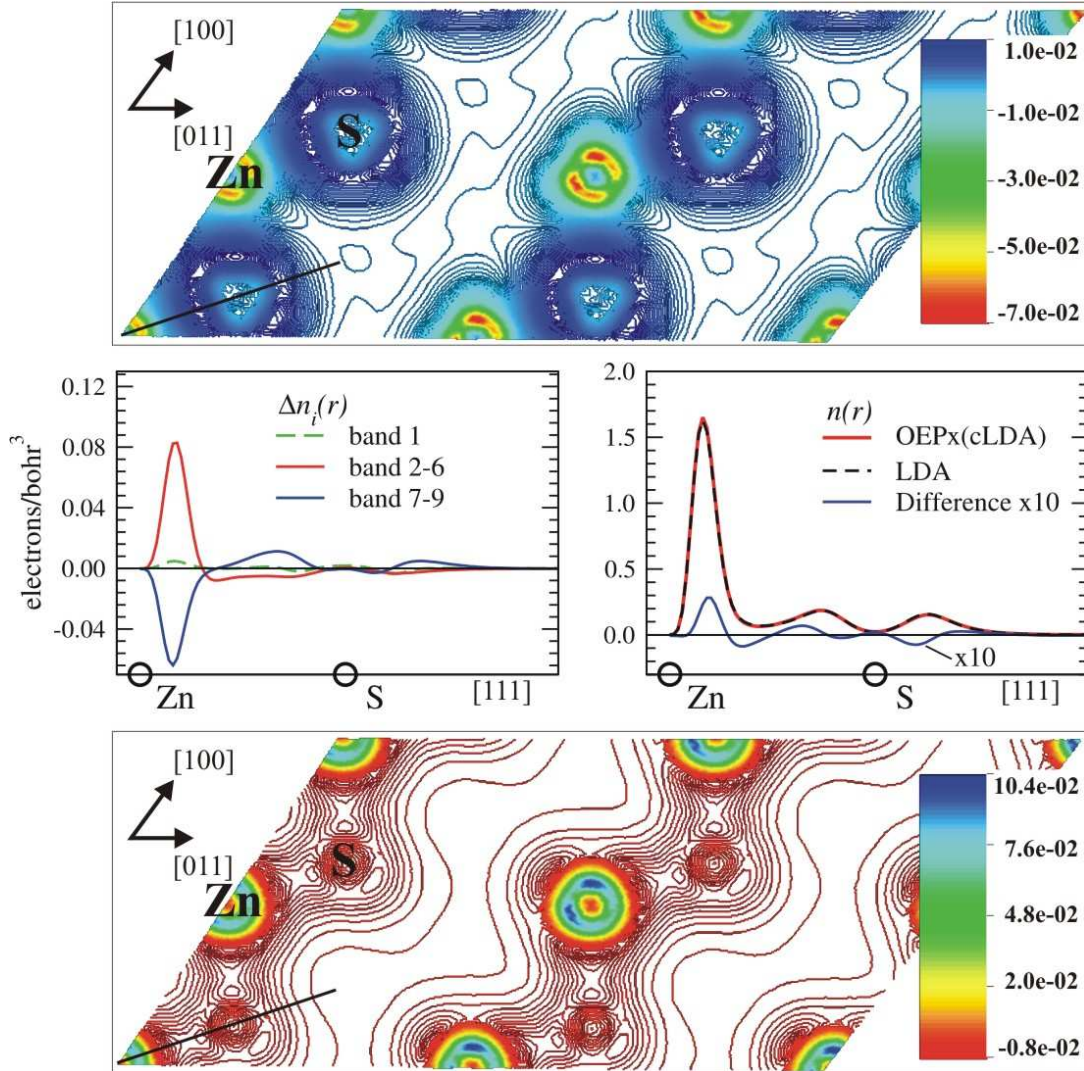
Figure 3. Comparison between OEPx(cLDA) and LDA results for the electron density and the partial densities difference ($\Delta n_i(\mathbf{r})$) of ZnS: Positive density differences indicate an accumulation in OEPx(cLDA). *Middle panel – left*: partial density differences along the [111] direction through the unit cell; while the s-band (green, dashed) remains largely unaffected, the d-electrons (red) are drawn from the valence region and are localised more strongly on the Zn atom, whereas the remaining valence electrons (blue) accumulate stronger in the bonding region in OEPx(cLDA). *Middle panel – right*: The OEPx(cLDA) (red, solid) and LDA (black, dashed) electron densities are almost indistinguishable. The density difference (blue line – magnified by a factor of 10) reflects the partial density changes. (The scale of the ordinate is the same as in Fig. 4.) Cross sections through the partial density difference in electrons/bohr^3 for valence bands (7-9) and d-bands (2-6) are displayed in the *top* and *bottom panel*, respectively. The path taken for the one-dimensional plots in the middle panels is marked by the black line.
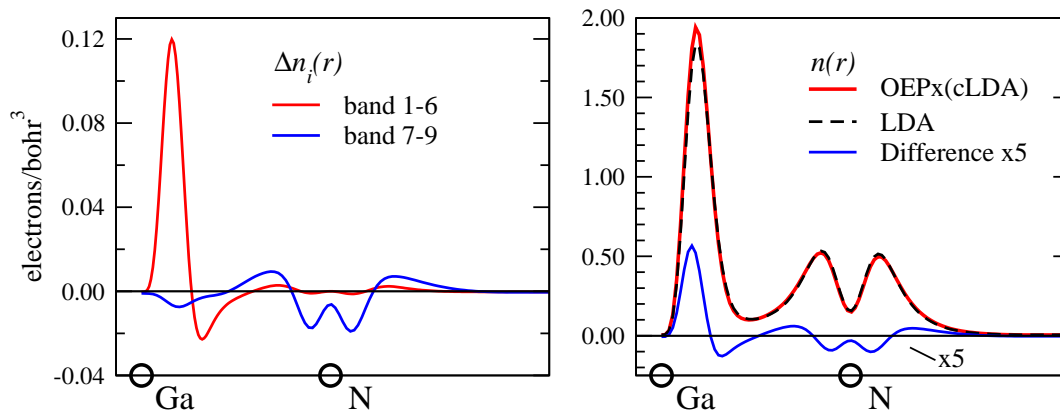
Figure 4. *Left hand side*: partial density differences ($\Delta n_i(\mathbf{r})$) along the [111] direction through the unit cell of GaN (same as Fig. 3). The d-electrons (red) localise stronger on the Ga atom, but are not drawn from the remaining valence electrons (blue) as in ZnS. *Right hand side*: The OEPx(cLDA) (grey) and LDA (black) electron densities are very similar. The density difference (red line – magnified by a factor of 5) reflects the stronger localisation of the d-electrons.

observed since the S $3s$ states remain almost unaffected by the change in the exchange-correlation potential. This behaviour is analogously found in ZnO and CdS.

In GaN on the other hand the d-states hybridise strongly with the N $2s$ states (shown together as red line) and are energetically separated from the remaining valence electrons (blue line). Again we observe a localisation of the d-electrons on the cation upon removal of the self-interaction. But this time the charge accumulation is not compensated by a reduction of the valence electrons, which were already bound closer to the N atom and are now shifted more into the bonding region by the OEPx(cLDA).

Previously it was observed that LDA densities are more homogeneous than their OEPx counterpart [19]. Furthermore, the OEPx density was found to localise stronger in the bonding region for GaAs and GaN [20]. In these calculations the d-electrons were frozen in the core of the pseudopotential. Although these observations certainly apply to the *upper valence* electrons our results show that the d-electrons introduce the opposite effect. This leads to a more pronounced electron localisation on the cation in GaN in the OEPx approach[11] and cancels out the charge accumulation in the bonding region in ZnO, ZnS and CdS.

In the following sections we will analyse the implications of these observations for the bandstructure of the four semiconductors and compare to spectroscopical data where available.

3.3.2. Band Gaps   Before we proceed with a more detailed analysis of the electronic structure for the selected II-VI compounds and group-III-nitrides in our approach we like to highlight one of our key results: *the OEPx(cLDA) based schemes systematically open the band gap compared to the LDA based variants*, as illustrated in Fig. 5. *Our GW bandstructure calculations reproduce the experimental values very well*[12] *when starting from the OEPx(cLDA) ground state.* In the

[11] The inclusion of LDA correlation in OEPx(cLDA) does not change these observations.
[12] For ZnO experimental data is only available for the wurtzite structure. On the level of LDA the band gap is 0.2 eV larger in wurtzite than in zinc-blende. To compare with the experimental data we have therefore adjusted all values for ZnO in Fig. 5 by this amount.
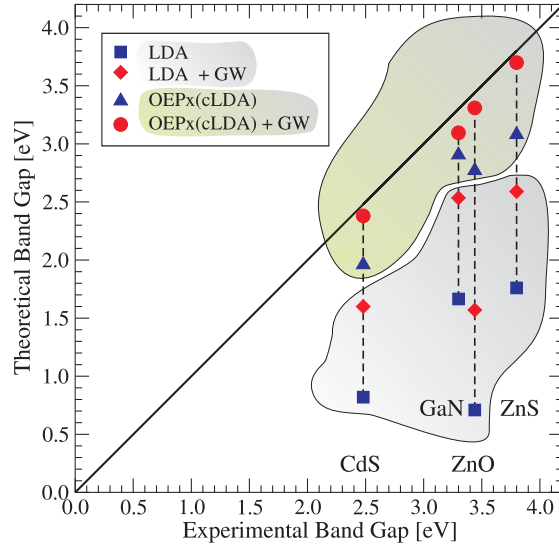
Figure 5. Theoretical versus experimental band gaps: the OEPx(cLDA) based schemes systematically open the band gap compared to the LDA based calculations. Our OEPx(cLDA)+GW calculations with the cation d-electrons included as valence electrons agree very well with the experimental values (see Tab. 3 for references). (For ZnO an estimate of 0.2 eV was added to the zinc-blende values in order to compare to the experimental results for wurtzite (see text).)

LDA based GW calculations on the other hand the band gaps are underestimated appreciably with the LDA itself giving the most severe underestimation [26, 27, 28].

3.3.3. II-VI Semiconductors In Fig. 6 we compare the four different computational approaches for the whole bandstructure of ZnS[13]. To facilitate a numerical comparison we have also listed the band gaps and d-electron binding energies in Tab. 3 and 4 together with the values for the other compounds.

We observe that the reduction of the p-d hybridisation due to the removal of the self-interaction in OEPx(cLDA) discussed in the previous section decreases the valence bandwith and a larger gap between the p and d bands is opened (right panel). The d-bands, however, remain almost in the same position as in the LDA. The GW valence bandstructure is very similar to the OEPx(cLDA) one, apart from small dispersive shifts in the p-band complex. The conduction bands are shifted up almost uniformly opening the fundamental band gap to 3.7 eV compared to the experimental value of 3.8 eV.

Starting from the LDA ground state, however, we find that in GW the d-bands overlap in energy with the p-bands (left panel). The reason for this unphysical behaviour can be traced back to the pseudopotential approximation. Since the atomic d-orbitals of Zn and Cd overlap considerably with the wavefunctions of the s and p electron in the same shell, the exchange interaction between the d and the remaining core electrons in this shell is strong. The poor performance of the LDA can thus largely be explained by spurious self-interaction effects, as alluded to before and demonstrated numerically by applying self-interaction corrections (SIC) [11, 12, 13, 126].

---

[13] The results for ZnS are representative for ZnO and CdS and we therefore only show bandstructure for ZnS.

In Fig. 7 we have plotted the quasiparticle corrections of ZnS and GaN as a function of the Kohn-Sham energy. If valence and conduction bands were shifted uniformly, as this is the case in Silicon for instance, the circles would form horizontal lines with a jump at the Fermi energy [78]. Instead the quasiparticle corrections to the upper valence states of the OEPx(cLDA) ground state decrease linearly with increasing energy. This leads to a change of the band dispersion in the quasiparticle bandstructure and we thus speak of *dispersive quasiparticle shifts*. The origin for the dispersive nature of the quasiparticle shift is still unclear and needs to be investigated in the future. The corrections to the LDA bandstructure of ZnS, however, exhibit two different features: one branch shows a similar dispersion than in the OEPx(cLDA)+GW case, whereas the corrections to the band that hybridises most strongly in energy with the d-electrons scatter wildy. This unphysical behaviour is a direct consequence of the inconsistent treatment of core-valence exchange in these pseudopotential LDA+GW calculations.
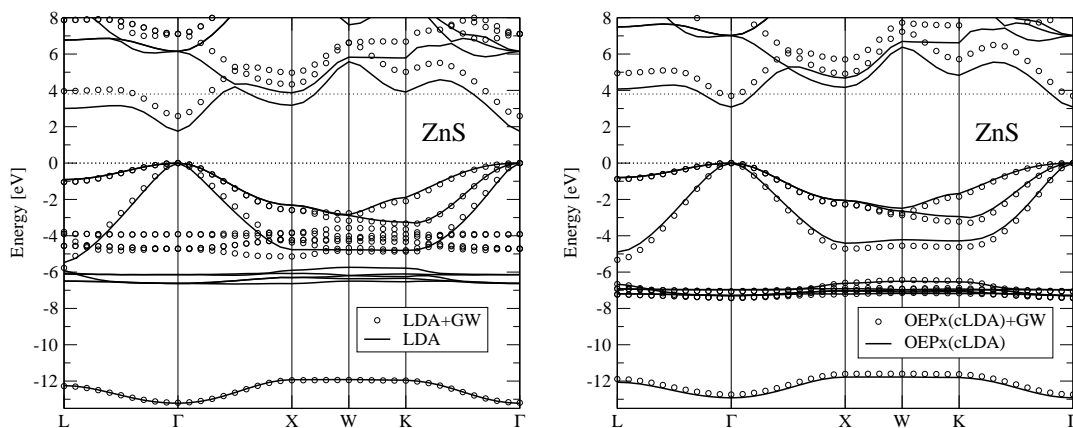

Figure 6. Band structure of ZnS in LDA and LDA+GW (panel on the left) compared with OEPx(cLDA) and OEPx(cLDA)+GW (panel on the right). Consistent pseudopotentials are used. All bandstructures have been aligned at the valence band maximum (dotted line at 0 eV). For reference the experimental band gap is marked by the 2nd dotted line.

For computational schemes that rely on core-valence partitioning it is therefore essential to capture the dominant part of core-valence exchange and correlation correctly. Retaining the s and p orbitals of the cation d-shell in the core of the pseudopotential will effectively freeze the core-valence interaction on the level of the density functional employed, i.e. here LDA or OEPx(cLDA). In the subsequent GW calculation, however, this interaction would be treated by the non-local, dynamic self-energy. Since the dominant contribution arises from core-valence exchange, the LDA is not particularly well suited to replace the self-energy. As a consequence the perturbation matrix $[\Sigma - v_{xc}]_{nm}$ becomes non-diagonal and equation (3.1) is no longer valid. As a result the d-bands are incorrectly shifted up into the upper valence bands (see left panel of Fig. 6) and the energy gap opens only by 0.8 eV to 1.60 eV. This effect was first observed by Rohlfing *et al.* [33] (see also line 13 in Tab. 3 and 10 in Tab. 4), who also noted that moving up to second-order perturbation theory in the solution of equation (3.1) gives only marginal improvements. In order to restore the exchange-interaction, the s and p electrons would have to be included as valence electrons in the GW calculation for the Fock part of the self-energy to take effect [33, 34, 35] (lines 14 and 15 in Tab. 3 and lines 11 and 12 in Tab. 4).

In the OEPx approach on the other hand exchange is treated exactly. Since we expect
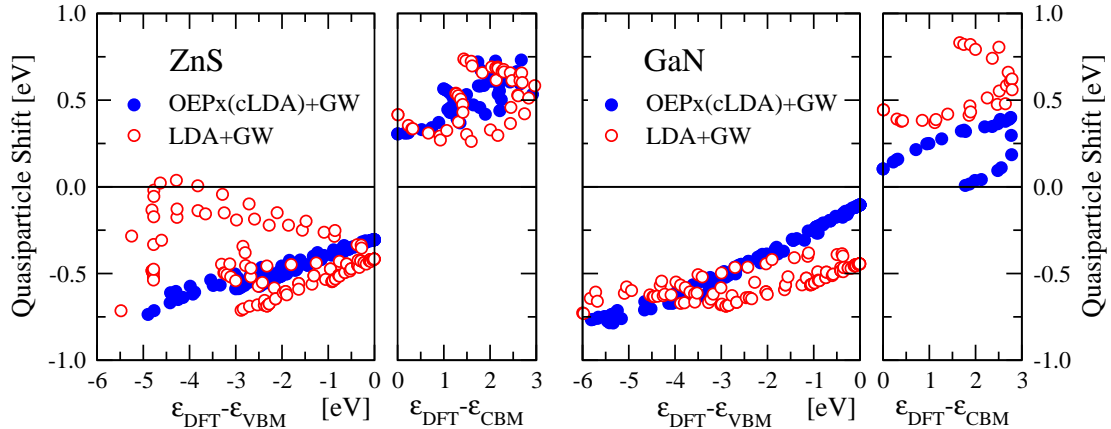
Figure 7. Quasiparticle shifts as function of the Kohn-Sham energy for ZnS and GaN for GW calculations based on an LDA (open circles) and an OEPx(cLDA) (filled circles) ground state. In order to avoid visual distortions due to the band gap difference between LDA and OEPx(cLDA) the curves have been aligned on the abscissa such that both the valence band maximum (VBM) and the conduction band minimum (CBM) are equal to zero. For both materials the quasiparticle corrections to the OEPx(cLDA) bandstructure are dispersive. In GaN this effect is slightly more pronounced than in ZnS. The corrections to the LDA bandstructure are less dispersive in GaN, but scatter strongly for ZnS (see text).

dynamic correlation effects to be small for core electrons, the dominant contribution is therefore captured by OEPx and we can retain the s and p core states in the frozen core of the pseudopotential. Indeed we observe that the improved description of the pseudoatoms obtained in OEPx(cLDA) (section 3.1) translates to the solids giving band gaps and d-electron binding energies systematically closer to experiment than in LDA+GW. Including LDA correlation increases the band gaps and d-electron binding energies only slightly by between 0.1 and 0.2 eV compared to OEPx (lines 5 and 6 in Tab. 3 and 4). While the GW formalism proves to be insensitive to this small variation for the band gaps (lines 7 and 8 in Tab. 3) the small shift carries over from OEPx+GW to OEPx(cLDA)+GW for the d-electron binding energies (lines 7 and 8 in Tab. 4).

For ZnS and CdS OEPx(cLDA) and OEPx(cLDA)+GW produce essentially the same d-electron binding energies. Only in ZnO quasiparticle corrections are found to lower the d-states by 1.5 eV compared to OEPx(cLDA), further reducing the p-d coupling. Overall the binding energies obtained with our OEPx(cLDA)+GW agree well with other available GW calculations (line 11, 12 and 14 in Tab. 4), but are still about 2 eV at variance with experiment. Previously Rohlfing *et al.* have devised a GW scheme in which plasmon satellites are included in the Green's function denoted here by SAT (line 13 in Tab. 4). Although the SAT improves on the d-electron binding energies the good agreement with experiment for the valence part of the bandstructure is lost [133]. Work towards a more elaborate theory that provides a description of both the upper valence part of the bandstructure and the d-bands in agreement with photoemssion data is clearly required in the future.

For completeness we have also included previous studies in Tab. 3 in which the d electrons were treated as part of the frozen core (lines 10-12). For reasons given in the previous section these calculations have to be interpreted cautiously because p-d and d-s hybridisation is

Table 3. DFT and quasiparticle band gaps in eV for ZnO, ZnS, CdS, and GaN in the zinc-blende structure sorted in increasing energy from top to the experimental values. The first column lists the DFT scheme and the second column denoted PP the pseudopotential used. For all-electron calculations this column denotes if the atomic sphere approximation (ASA) or the full potential (FP) was employed. "Conf." refers to the configurations of the (pseudo)atoms: d-electrons included (d), as described in the previous section, valence only (no d's), d-electrons and their respective shell included (d-shell) and all-electron (all e^-). Experimental results are taken from: ZnO [127], ZnS [128], CdS [129], GaN [130] and the OEPx(cLDA) and GW data from: [a]Ref. [131], [b]Ref. [132], [c]Ref. [23], [d]Ref. [18], [e]Ref. [20], [f]Ref. [33], [g]Ref. [35], [h]Ref. [34], [i]Ref. [30], [j]Ref. [29], [k]Ref. [98], [l]Ref. [99]. The superscript [w] denotes wurtzite structures. In Ref. [a] and [b] a model dielectric function was employed and in Ref. [e,f,g,h] a plasmon pole model was used.

	DFT	PP	Conf.	GW	ZnO	ZnS	CdS	GaN
1	LDA	LDA	d			0.51	1.76	0.81	1.65
2	OEPx(cLDA)	LDA	d			1.34	2.19	1.34	2.55
3	LDA	LDA	d	GW	1.36	2.59	1.60	2.54
4	OEPx(cLDA)	LDA	d	GW	2.03	2.65	1.71	2.87
5	OEPx	OEPx	d		2.34	2.94	1.84	2.76
6	OEPx(cLDA)	OEPx(cLDA)	d		2.57	3.08	1.96	2.88
7	OEPx	OEPx	d	GW	3.07	3.62	2.36	3.09
8	OEPx(cLDA)	OEPx(cLDA)	d	GW	3.11	3.70	2.39	3.09
9	Experiment				3.44[w]	3.80	2.48	3.30
10	LDA	LDA	no d's	GW		3.98[a]	2.83[a]	3.10[b]
11	OEPx(cLDA)	OEPx(cLDA)	no d's			3.74[c]		3.46[d]
12	OEPx(cLDA)	OEPx(cLDA)	no d's	GW				3.49[e]
13	LDA	LDA	d	GW			1.50[f]	
14	LDA	LDA	d-shell	GW		3.64[g]		
15	LDA	LDA	d-shell	GW		3.50[h]	2.45[h]	2.88[h]
16	LDA	FP	all e^-	GW	2.44[w,i]	3.24[j]		3.03[w,j]
17	LDA	ASA	all e^-	GW	4.06[w,l]	3.97[k]		3.25[w,l]

completely absent.

Existing full-potential all-electron LDA+GW calculations (line 16) report band gaps to within 0.5 to 0.6 eV for GaN and ZnS, but are more at variance for ZnO. An underestimation in the RPA dielectric screening resulting from the LDA ground state was given as a possible explanation for this discrepancy in Ref. [30]. The change in density and wavefunctions from LDA to OEPx(cLDA) (see previous sections) is also likely to be an important factor, which requires further analysis. Recently this conjecture was substantiated by an approximate self-consistent GW scheme in which new ground state wavefunctions and a new ground state density were calculated from a static but non-local self-energy at every iteration step [32]. Earlier all-electron calculations in the atomic sphere approximation (ASA) to LMTO were also included in Tab. 3 and 4 (lines 15 and 17, respectively). The restriction of the potential to a spherical shape inside the atomic spheres together with the omission of interstitial plane waves in the LMTO leads to an overestimation of band gaps and d-electron binding energies in the ASA. The seemingly good agreement with experiment for ZnS and GaN, however, is therefore fortuitous as the comparison with the more sophisticated full-potential LAPW calculations in the lines above illustrates.

To emphasize the importance of consistency concerning the choice of the exchange-

Table 4. d-electron binding energies referenced to the top of the valence band: The layout is the same as in Table 3. Experimental values taken from: [a]Ref. [89], [b]Ref. [90], [c]Ref. [91], and the GW data from: [d]Ref. [33], [e]Ref. [35], [f]Ref. [34], [g]Ref. [133], [h]Ref. [30], [i]Ref. [29], [j]Ref. [99], [k]Ref. [98]. SAT denotes GW calculations including plasmon satellites and the superscript [w] markes studies on the wurtzite structure. In Ref. [d,e,f] a plasmon pole model was used.

	DFT	PP	Conf.	GW	ZnO	ZnS	CdS	GaN
1	LDA	LDA	d	GW	4.29	4.30	6.17	13.05
2	OEPx(cLDA)	LDA	d	GW	4.98	5.02	6.40	13.58
3	OEPx(cLDA)	LDA	d		4.36	5.33	6.54	12.75
4	LDA	LDA	d		5.20	6.32	7.72	14.25
5	OEPx	OEPx	d		5.12	6.91	7.57	14.85
6	OEPx(cLDA)	OEPx(cLDA)	d		5.20	7.05	7.61	15.02
7	OEPx	OEPx	d	GW	6.68	6.97	7.66	16.12
8	OEPx(cLDA)	OEPx(cLDA)	d	GW	6.87	7.08	7.75	16.15
9	Experiment				$9.00^{w,a}$	8.97^a 9.03^b	9.50^b	17.70^c
10	LDA	LDA	d	GW			5.20^d	
11	LDA	LDA	d-shell	GW		7.40^e		
12	LDA	LDA	d-shell	GW		6.40^f	8.10^f	15.70^f
13	LDA	LDA	d-shell	SAT		7.90^f	9.10^g	17.30^f
14	LDA	FP	all e^-	GW	6.16^h	7.10^i	8.20^i	$16.40^{w,i}$
15	LDA	ASA	all e^-	GW	$5.94^{w,j}$	8.33^k		$17.60^{w,j}$

correlation functional in the pseudopotential generation and subsequent bulk calculation we found it illuminating to include a hybrid calculation in our analysis. Line 2 in Tab. 3 list the values of an OEPx(cLDA) calculation carried out with LDA pseudopotentials. The gap increases over the LDA values but falls short of the LDA+GW results. Even more illuminating are the results of the OEPx(cLDA)+GW hybrid calculation (line 4), which only marginally improve on the LDA+GW scheme, jeopardizing the good agreement achieved with OEPx(cLDA) pseudopotenials. This is due to the fact that the self-interaction frozen in the LDA pseudopotential pushes the d-electrons up to the valence bands (line 3 in Tab. 4) effectively closing the p-d gap. The resulting bandstructure looks similar to the LDA+GW bandstucture in Fig. 6 giving little to no improvement on the LDA results.

Contrary to the LDA, the exchange potential in OEPx is constructed to best reproduce the exchange part of the self-energy. OEPx and OEPx(cLDA) can therefore be regarded as the better and more consistent ground state for a GW excited states calculation for these systems. This conjecture is corroborated by the numerical results given in Tab. 3 and 4. Summarising the hierachy that has emerged for the computational schemes presented here, we find all schemes based on LDA pseudopotentials at the top of the table and therefore to be the least accurate. We conclude that using OEPx(cLDA) pseudopotentials in our approach is essential. But despite the considerably opening of the band gaps in the OEPx(cLDA) calculations for the four compounds, many-body perturbation theory in the GW quasiparticle approximation is needed to achieve a good description of the excitation spectrum and, hence, good agreement with spectroscopy data.

3.3.4. Group-III-Nitrides: GaN As an example for the group-III-nitrides we only consider GaN in this article, whose bandstructure in our different computational schemes is shown in
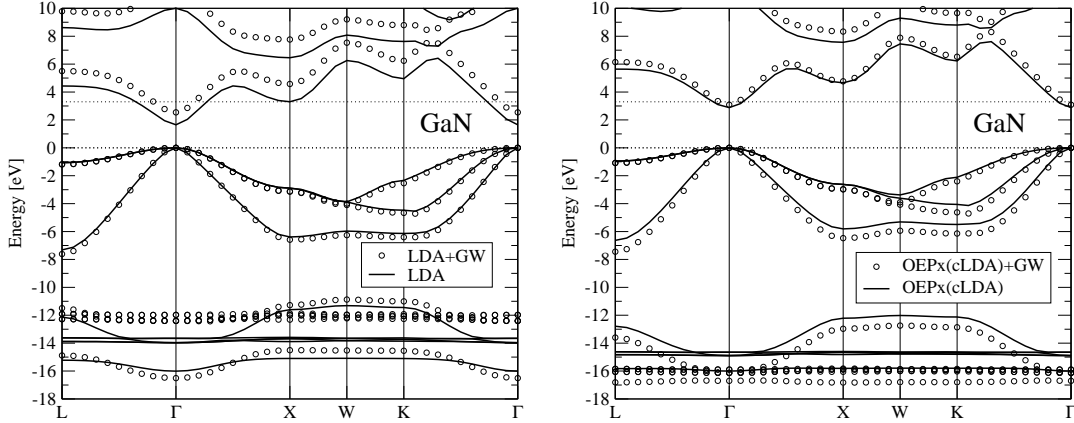
Figure 8. Band structure of GaN in LDA and LDA+GW (panel on the left) compared with OEPx(cLDA) and OEPx(cLDA)+GW (panel on the right). Consistent pseudopotentials are used. All bandstructures have been aligned at the valence band maximum (dotted line at 0 eV). For reference the experimental band gap is marked by the 2nd dotted line.

Fig. 8. Values for the band gaps and the d-electron binding energies [14] have been included in Tab. 3 and 4. The bandstructure of GaN clearly reflects the enhanced s-d coupling while the p-d coupling is greatly reduced compared to the II-VI semiconductors. As a consequence the upper valence bands are very similar in all four computational schemes. The removal of self-interaction in the OEPx(cLDA) based approach (right panel) shifts all conduction states to higher energies compared to the LDA (left panel), opening the band gap by 1.2 eV [25]. The self-energy corrections in the OEPx(cLDA)+GW calculations, however, are not as pronounced as for the II-VI semiconductors. This is due to the fact that the d-electrons are much lower in energy and more strongly localised on the cation and hence do not contribute as much to the correlation part of the self-energy as in the case of the II-VI compounds. The Ga d and N s bands in our OEPx(cLDA)+GW are in very good agreement with GW calculations by Rohlfing *et al.* [34] with small differences only at the Γ-point.

The quasiparticle shifts to the LDA ground state are dispersionless for the lower conduction bands, as Fig. 7 illustrates, but scatter in an energy window of ± 0.2 eV around a value of -0.6 eV for the upper valence states. The self-energy correction to the OEPx(cLDA) ground state on the other hand decreases almost linearly with increasing energy and is thus much more dispersive than for the LDA ground state (compare also the left and right panel of Fig. 8).

It remains to be added that all statements made in the previous section about the comparison between the OEPx and OEPx(cLDA) results and those of the respective GW calculations also hold true for GaN. For the OEPx(cLDA) hybrid approach with LDA pseudopotentials we observe two different regimes. Due to the reduced p-d coupling in GaN, the removal of the self-interaction among the valence electrons leads to small improvements for the band gap in the OEPx(cLDA) compared to the LDA results (lines 2 and 4 in Tab. 3). The Ga $3d$ binding energies and the dispersion of the semicore bands, however, are comparable to those in the LDA (lines 2 and 4 in Tab. 4).

---

[14] The center of the d-bands for GaN has been obtained by averaging over the lowest five bands at the Γ-point only.

3.3.5. Electronic Self-Energy We will close our investigation into the electronic structure of the four compounds presented here with an analysis of the electronic self-energy. Since we apply *GW* non-self consistently as a perturbation to the Kohn-Sham bandstructure ($\{\epsilon_{n\mathbf{k}}^{\mathrm{DFT}}\}$) without diagonalising the quasiparticle Hamiltonian the quasiparticle energies ($\{\epsilon_{n\mathbf{k}}^{qp}\}$) comprise four contributions[15]

$$\epsilon_{n\mathbf{k}}^{qp} = \epsilon_{n\mathbf{k}}^{\mathrm{DFT}} + \langle \phi_{n\mathbf{k}} | \Sigma_{xc}^{GW}(\epsilon_{n\mathbf{k}}^{qp}) - v_{xc} - \Delta\mu | \phi_{n\mathbf{k}} \rangle \quad . \tag{3.2}$$

A closer look at equation (3.2) reveals that the quasiparticle energies can change because a) the Kohn-Sham bandstructure to which the self-energy corrections are applied changes b) the ingredients (Kohn-Sham energies and wavefunctions) for the self-energy operator have changed and/or c) because the wavefunctions used for the evaluation of the matrix elements in equation (3.2) differ from one ground state to another.

To ascertain which of these three factors dominantes we have compiled the individual contributions[16] that enter equation (3.2) in Table 5 for three selected states of ZnS and GaN. In order to isolate the influence of the Kohn-Sham bandstructure it is conducive to separated the perturbation $\langle \Sigma - v_{xc} \rangle$ into a static $\langle \Sigma_x - v_{xc} \rangle$ and a dynamic[17] $\langle \Sigma_c(\epsilon^{qp}) \rangle$ contribution evaluated at the converged quasiparticle energy. The static part depends only on the wavefunctions of the occupied states (see equation (2.17)) and the wavefunction of the bandstructure state for which the quasiparticle energy is evaluated, whereas the correlation part of the self-energy is additionally dependent on the wavefunctions of all unoccupied states and the Kohn-Sham eigenvalues via the dynamic polarisability (see equation (2.12) to (2.18)).

Focusing first on the conduction band minimum (CBM) and the valence band maximum (VBM) of ZnS and GaN we observe that the correlation contributions of the self-energy agree to within 0.05 eV for the respective states and thus prove to be insensitive to changes in the ground state from LDA to OEPx(cLDA). The same is true for the static contribution, which changes up to only 0.3 eV, although both $\langle \Sigma_x \rangle$ and $\langle v_{xc} \rangle$ taken individually exhibit larger variations. This pattern is transferable to the other upper valence and conduction states and to ZnO and CdS. From this we conclude that the perturbation $\langle \Sigma - v_{xc} \rangle$ is small for this part of the energy spectrum and largely insensitive to variations in the exchange-correlation functional from LDA to exact-exchange in the II-VI compounds. In GaN the difference in the quasiparticle shifts between the two *GW* calculations is more pronounced (see also Fig. 7) but with ∼0.7 eV still amounts to only half of the band gap difference between LDA and OEPx(cLDA). The strong improvement we have reported in the previous sections for the OEPx(cLDA)+*GW* approach is therefore, to a large extend, due to the changes in the Kohn-Sham bandstructure.

For the *d*-bands, however, the situation is drastically different. The correlation contribution is still very similar with differences around 0.3 eV, but the static contribution differs vastly by up to 2.5 eV for the case of GaN. In addition the perturbation operator is no longer diagonal in the LDA+*GW* calculations [33, 35] and the *d*-bands are pushed upwards into the upper valence states in the II-VI compounds [33] (see Fig. 6). This is a direct consequence of the inconsistent description of core-valence exchange for the cation in the LDA+*GW* approach. We therefore expect that in full-shell LDA+*GW* calculations the static contribution for the *d*-electrons becomes comparable in size to the values for our OEPx(cLDA)+*GW* calculations in which core-valence exchange is treated much more consistently through the OEPx pseudopotentials. At the same time this modified exchange self-energy will affect the perturbation operator for

---

[15] For clarity we have repeated equation (3.1) here.

[16] For the remainder of the discussion we have introduced $\langle A \rangle$ as a short hand notation for the matrix elements $\langle \phi_{n\mathbf{k}} | A | \phi_{n\mathbf{k}} \rangle$. The alignment constant $\Delta\mu$ has been absorbed into the matrix elements of v_{xc}.

[17] The distinction between *static* and *dynamic* is made here purely on the grounds of distinguishing between explicitly energy dependent (dynamic) and energy independent quantities (static). It is not to be understood in the quantum chemical sense as the difference between Hartree-Fock and dynamic correlation methods.

Table 5. Contributions to the quasiparticle energy shift as applied via equation (3.2) for ZnS and GaN and three different representative states: the conduction band minimum (CBM), the valence band maximum (VBM) and the highest (lowest) d-electron state for Zns (GaN) at the Γ-point (d-state). The columns list the DFT eigenvalues (ϵ^{DFT}) for the respective ground state (GS) calculation, the matrix elements of the exchange part ($\langle \Sigma_x \rangle$, equation (2.17)) and the correlation part ($\langle \Sigma_c \rangle$, equation (2.18)) of the self-energy, the matrix elements of the exchange-correlation potential ($\langle v_{xc} \rangle$, including the alignment constant $\Delta \mu$ (equation (3.1))) and the static contribution ($\langle \Sigma_x - v_{xc} \rangle$). (All energies are given in eV).

	State	GS	ϵ^{DFT}	$\langle \Sigma_x \rangle$	$\langle v_{xc} \rangle$	$\langle \Sigma_c \rangle$	$\langle \Sigma_x - v_{xc} \rangle$
ZnS	CBM	LDA	1.75	−7.14	−11.82	−4.33	4.68
		OEPx(cLDA)	3.08	−6.56	−11.26	−4.39	4.69
	VBM	LDA	0.00	−17.64	−15.60	1.62	−2.04
		OEPx(cLDA)	0.00	−17.60	−15.73	1.57	−1.87
	d-state	LDA	−6.62	−28.19	−24.74	4.95	−3.46
		OEPx(cLDA)	−7.29	−29.01	−23.29	5.27	−5.71
GaN	CBM	LDA	1.65	−10.05	−14.76	−4.27	4.72
		OEPx(cLDA)	2.88	−9.23	−13.61	−4.28	4.38
	VBM	LDA	0.00	−21.15	−18.40	2.32	−2.76
		OEPx(cLDA)	0.00	−21.45	−19.03	2.32	−2.43
	d-state	LDA	−13.97	−31.77	−27.40	5.19	−4.37
		OEPx(cLDA)	−14.89	−32.46	−25.61	5.50	−6.85

the valence states much more, which then leads to a lowering of the occupied states relative to the conduction states and thus to the opening of the band gap that is observed in full-shell [33, 34, 35, 131] and all-electron [29, 30, 32] LDA+GW calculations. A numerical verification of this hypothesis will be given elsewhere.

4. Conclusions

We have reported a first combined OEPx and GW study investigating the effects of semicore states on the electronic structure of selected II-VI compounds and group-III-nitrides. The removal of the self-interaction in the OEPx(cLDA) approach leads to a stronger localisation of the cation d-electrons compared to the LDA and thus to a reduced p-d hybridisation. As a result both the gap between d and upper valence bands as well as between valence and conduction bands opens up in the OEPx(cLDA) approach. Switching to the GW picture of interacting quasiparticles we obtain band gaps in very good agreement with photo-electron spectroscopy, provided of course we start from an OEPx or OEPx(cLDA) ground state.

The self-energy correction shifts the conduction and upper valence bands almost rigidly when starting from an LDA calculation, whereas in the case of OEPx(cLDA) ground states the corrections are dispersive. Dispersive self-energy shifts are relatively uncommon and not frequently reported in the literature; a point that requires further investigation in the future.

We find that the d-electron binding energies in our OEPx(cLDA)+GW approach are in good agreement with those of previously reported GW calculations but are still at variance with experiment. The fact that the erroneous energetical position of the d-electrons actually produces quasiparticle energies for the upper valence and conduction bands in agreement with experiment indicates that the GW approximation might not suffice to fully describe the strongly

localised cation d-electrons. A more elaborate theory incorporating electron-hole and/or vertex corrections might be necessary in order to obtain a bandstructure consistent with photo-electron spectroscopy over a larger energy window.

Consistency in the choice of the pseudopotential was found to be paramount. Moreover, employing OEPx(cLDA) pseudopotentials allows us to remove the s and p electrons of the respective d-shell from the calculation by freezing them in the core of the pseudopotential. This reduces the required plane-wave cutoff and thus the computational costs of our calculations tremendously. It remains to be verified, however, how the pseudoisation of the atomic wavefunctions affects the exchange-integrals in the OEPx approach. This will be the subject of future studies.

Furthermore we have alluded to the formal connection between the exchange potential in the OEPx formalism and the exchange part of the self-energy. Our numerical results confirm the hypothesis that for the class of materials presented here the DFT exact-exchange ground state constitutes a much better starting point for GW bandstructure calculations. In light of this we like to conclude with the outlook that the Sham-Schlüter equation (2.29) offers a formal but heuristic perspective to include quasiparticle correlation into the OEP ground state and thus to go beyond OEPx+GW.

Acknowledgements

References

[1] F. J. Himpsel, Adv. Physics **32**, 1 (1983).

[2] E. W. Plummer and W. Eberhardt, Adv. Chem. Phys. **49**, 533 (1982).

[3] L. Kevan, editor, *Angle-Resolved Photoemission*, Elsevier, Amsterdam, 1992.

[4] V. Dose, Surface Science Reports **5**, 337 (1985).

[5] N. V. Smith, Rep. Prog. Phys. **51**, 1227 (1988).

[6] J. C. Fuggle and J. E. Inglesfield, editors, *Unoccupied Electronic States*, Springer-Verlag, 1992.

[7] L. Hedin, Phys. Rev. **139**, A796 (1965).

[8] G. Onida, L. Reining, and A. Rubio, Rev. Mod. Phys. **74**, 601 (2002).

[9] W. G. Aulbur, L. Jönsson, and J. W. Wilkins, Solid State Phys. : Advances in Research and Applications **54**, 1 (2000).

[10] F. Aryasetiawan and O. Gunnarsson, Rep. Prog. Phys. **61**, 237 (1998).

[11] D. Vogel, P. Krüger, and J. Pollmann, Phys. Rev. B **52**, R14316 (1995).

[12] D. Vogel, P. Krüger, and J. Pollmann, Phys. Rev. B **54**, 5495 (1996).

[13] D. Vogel, P. Krüger, and J. Pollmann, Phys. Rev. B **55**, 12836 (1997).

[14] T. Kotani, Phys. Rev. B **50**, 14816 (1994), *ibid.* **51**, 13903(E) (1995).

[15] T. Kotani, Phys. Rev. Lett. **74**, 2989 (1995).

[16] T. Kotani and H. Akai, Phys. Rev. B **54**, 16502 (1996).

[17] A. Görling, Phys. Rev. B **53**, 7024 (1996).

[18] M. Städele, J. A. Majewski, P. Vogl, and A. Görling, Phys. Rev. Lett. **79**, 2089 (1997).

[19] M. Städele, M. Moukara, J. A. Majewski, P. Vogl, and A. Görling, Phys. Rev. B **59**, 10031 (1999).

[20] W. G. Aulbur, M. Städele, and A. Görling, Phys. Rev. B **62**, 7121 (2000).

[21] A. Fleszar, Phys. Rev. B **64**, 245204 (2001).

[22] D. Gall, M. Städele, K. Järrendahl, I. Petrov, P. Desjardins, R. T. Haasch, T.-Y. Lee, and J. E. Greene, Phys. Rev. B **63**, 125119 (2001).

[23] N. Fitzer, A. Kuligk, R. Redmer, M. Städele, S. M. Goodnick, and W. Schattke, Phys. Rev. B **67**, R201201 (2003).

[24] R. J. Magyar, A. Fleszar, and E. K. U. Gross, Phys. Rev. B **69**, 045111 (2004).

[25] A. Qteish, A. I. Al-Sharif, M. Fuchs, M. Scheffler, S. Boeck, and J. Neugebauer, to be published.

[26] V. Fiorentini, M. Methfessel, and M. Scheffler, Phys. Rev. B **47**, 13353 (1993).

[27] P. Schröer, P. Krüger, and J. Pollmann, Phys. Rev. B **47**, 6971 (1992).

[28] P. Schröer, P. Krüger, and J. Pollmann, Phys. Rev. B **48**, 18264 (1993).

[29] T. Kotani and M. van Schilfgaarde, Solid State Commun. **121**, 461 (2002).

[30] M. Usuda, N. Hamada, T. Kotani, and M. van Schilfgaarde, Phys. Rev. B **66**, 125101 (2002).

[31] M. Usuda, N. Hamada, K. Shiraishi, and A. Oshiyama, Jpn. J. Appl. Phys. **43**, L407 (2004).

[32] S. V. Faleev, M. van Schilfgaarde, and T. Kotani, Phys. Rev. Lett. **93**, 126406 (2004).

[33] M. Rohlfing, P. Krüger, and J. Pollmann, Phys. Rev. Lett. **75**, 3489 (1995).

[34] M. Rohlfing, P. Krüger, and J. Pollmann, Phys. Rev. B **57**, 6485 (1998).

[35] W. Luo, S. Ismail-Beigi, M. L. Cohen, and S. G. Louie, Phys. Rev. B **66**, 195215 (2002).

[36] M. Moukara, M. Städele, J. A. Majewski, P. Vogl, and A. Görling, J. Phys. Condens. Matter **12**, 6783 (2000).

[37] E. Engel, A. Höck, R. N. Schmid, R. M. Dreizler, and N. Chetty, Phys. Rev. B **64**, 125111 (2001).

[38] C. O. Almbladh and L. Hedin, in *Handbook on Synchroton Radiation* edited by E. E. Koch (North Holland, 1983), volume 1, pp. 607–904.

[39] W. Bardyszewski and L. Hedin, Physica Scripta **32**, 439 (1985).

[40] J. E. Inglesfield, Physica Scripta **T17**, 89 (1987).

[41] L. Hedin and S. Lundqvist, in *Solid State Physics* edited by H. Ehrenreich, F. Seitz and D. Turnbull (Academic, New York, 1969), volume 23, p. 1.

[42] E. Gross, E. Runge, and O. Heinonen, *Many-Particle Theory*, Adam Hilger, 1991.

[43] L. D. Landau, Sov. Phys. JETP **3**, 920 (1957); *ibid.* **5**, 101 (1957); *ibid.* **35**, 70 (1959); L. D. Landau and E. M. Lifschitz, *Statistical Physics Part II* (Pergamon, Oxford).

[44] J. W. Gadzuk, in *Photoemission and Electronic Properties of Surfaces* edited by B. Feuerbach, B. Fitton and R. F. Willis (Wiley Interscience, 1978), pp. 111–136.

[45] J. D. Lee, O. Gunnarsson, and L. Hedin, Phys. Rev. B **60**, 8034 (1999).

[46] L. Hedin, J. Phys.: Condens. Matter **11**, R489 (1999).

[47] J. J. Rehr and R. C. Albers, Rev. Mod. Phys. **72**, 621 (2000).

[48] R. Hora and M. Scheffler, Phys. Rev. B **29**, 692 (1984).

[49] M. Bovet, V. N. Strocov, F. Clerc, C. Koitzsch, D. Naumović, and P. Aebi, Phys. Rev. Lett. **93**, 107601 (2004).

[50] V. N. Strocov, R. Claessen, G. Nicolay, S. Hüfner, A. Kimura, A. Harasawa, S. Shin, A. Kakizaki, P. O.

Nilsson, H. I. Starnberg, and P. Blaha, Phys. Rev. Lett. **81**, 4943 (1998).

[51] A. Schindlmayr, P. García-González, and R. W. Godby, Phys. Rev. B **64**, 235106 (2001).

[52] B. Holm and U. von Barth, Phys. Rev. B **57**, 2108 (1998).

[53] P. P. García-González and R. W. Godby, Phys. Rev. B **63**, 075112 (2001).

[54] K. Delaney, P. García-González, A. Rubio, P. Rinke, and R. W. Godby, Phys. Rev. Lett. **93**, 249701 (2004).

[55] W.-D. Schöene and A. G. Eguiluz, Phys. Rev. Lett. **81**, 1662 (1998).

[56] D. Tamme, R. Schepe, and K. Henneberger, Phys. Rev. Lett. **83**, 241 (1999).

[57] W.-D. Schöene and A. G. Eguiluz, Phys. Rev. Lett. **83**, 242 (1999).

[58] W. Ku and A. G. Eguiluz, Phys. Rev. Lett. **89**, 126401 (2002).

[59] M. L. Tiago, S. Ismail-Beigi, and S. G. Louie, Phys. Rev. B **69**, 125212 (2003).

[60] P. Hohenberg and W. Kohn, Phys. Rev. **136**, B864 (1964).

[61] W. Kohn and K. J. Sham, Phys. Rev. **140**, A1133 (1965).

[62] A. Görling and M. Levy, Phys. Rev. A, **50**, 196 (1994); *ibid.* Phys. Rev. B, **47**, 13105 (1993).

[63] C. Almbladh and U. von Barth, Phys. Rev. B **31**, 3231 (1985).

[64] M. Levy, J. P. Perdew, and V. Sahni, Phys. Rev. A **30**, 2745 (1984).

[65] M. E. Casida, Phys. Rev. B **59**, 4694 (1999).

[66] J. F. Janak, Phys. Rev. B **18**, 7165 (1978).

[67] O. V. Grisenko and E. J. Baerends, J. Chem. Phys., **120**, 8364 (2004); *ibid.* J. Chem. Phys., **117**, 9154 (2002); D. P. Chong, O. V. Grisenko and E. J. Baerends J. Chem. Phys., **116**, 1760 (2002); O. V. Grisenko, B. Braïda and E. J. Baerends J. Chem. Phys., **119**, 1937 (2003);.

[68] A. Savin, C. J. Umrigar, and X. Gonze, Chem. Phys. Lett. **288**, 391 (1998).

[69] J. Perdew and M. Levy, Phys. Rev. Lett. **51**, 1884 (1983).

[70] L. Sham and M. Schlüter, Phys. Rev. Lett. **51**, 1888 (1983).

[71] J. B. Krieger, Y. Li, and G. J. Iafrate, Phys. Rev. B **45**, 101 (1992).

[72] L. Sham and M. Schlüter, Phys. Rev. B **32**, 3883 (1985).

[73] M. E. Casida, Phys. Rev. A **51**, 2005 (1995).

[74] R. Grabo, T. Kreibich, S. Kurth, and E. K. U. Gross, in *Strong Coulomb Correlations in Electronic Structure Calculations: Beyond the Local Density Approximation* edited by V. I. Anisimov (Gordon and Breach, New York, 2000), volume 1, pp. 203–311.

[75] Y. M. Niquet, M. Fuchs, and X. Gonze, J. Chem. Phys. **118**, 9504 (2003).

[76] E. Engel, in *A Primer in Density-Functional Theory* edited by C. Fiolhais, F. Nogueira and M. Marques (Springer, Berlin, 2003), pp. 56–122.

[77] R. W. Godby, M. Schlüter, and L. J. Sham, Phys. Rev. Lett. **56**, 2415 (1986).

[78] R. W. Godby, M. Schlüter, and L. J. Sham, Phys. Rev. B **37**, 10159 (1988).

[79] R. T. Sharp and G. K. Horton, Phys. Rev. **90**, 317 (1953).

[80] J. D. Talman and W. F. Shadwick, Phys. Rev. A **14**, 36 (1976).

[81] S. Ivanov and M. Levy, J. Chem. Phys. **119**, 7087 (2003).

[82] J. Perdew and A. Zunger, Phys. Rev. B **23**, 5048 (1981).

[83] D. Ceperley and B. Alder, Phys. Rev. Lett. **45**, 566 (1980).

[84] A. Seidl, A. Görling, P. Vogl, J. A. Majewski, and M. Levy, Phys. Rev. B **53**, 3764 (1996).

[85] D. M. Bylander and L. Kleinman, Phys. Rev. B **41**, 7868 (1990).

[86] J. Lento and R. M. Nieminen, J. Phys.: Condens. Matter **15**, 4387 (2003).

[87] M. Kim, Y.-J. Zhao, A. J. Freeman, and W. Mannstadt, Appl. Phys. Lett. **84**, 3579 (2004).

[88] M. S. Hybertsen and S. G. Louie, Phys. Rev. B **34**, 5390 (1986).

[89] R. Weidemann, H.-E. Gumlich, M. Kupsch, H.-U. Middelmann, and U. Becker, Phys. Rev. B **45**, 1172 (1992).

[90] L. Ley, R. A. Pollak, F. R. McFeely, S. P. Kowalczyk, and D. A. Shirley, Phys. Rev. B **9**, 600 (1974).

[91] S. A. Ding, G. Neuhold, J. H. Weaver, P. Häberle, K. Horn, O. Brandt, H. Yang, and K. Ploog, J. Vac. Sci. Technol. A **14**, 819 (1996).

[92] E. L. Shirley, R. M. Martin, G. B. Bachelet, and D. M. Ceperley, Phys. Rev. B **42**, 5057 (1990).

[93] Y. Lee and R. J. Needs, Phys. Rev. B **67**, 035121 (2003).

[94] E. L. Shirley and R. M. Martin, Phys. Rev. B **47**, 15413 (1993), and references therein.

[95] E. L. Shirley, X. Zhu, and S. G. Louie, Phys. Rev. B **56**, 6648 (1997).

[96] F. Aryasetiawan and O. Gunnarsson, Phys. Rev. Lett. **74**, 3221 (1995).

[97] F. Aryasetiawan and O. Gunnarsson, Phys. Rev. B **54**, 17564 (1996).

[98] M. Oshikiri and F. Aryasetiawan, Phys. Rev. B **60**, 10754 (1999).

[99] M. Oshikiri and F. Aryasetiawan, J. Phys. Soc. Jap. **69**, 2113 (2000).

[100] B. Arnaud and M. Alouani, Phys. Rev. B **62**, 4464 (2000).

[101] S. Lebégue, B. Arnaud, M. Alouani, and P. Bloechl, Phys. Rev. B **67**, 155208 (2003).

[102] B. Králik, E. K. Chang, and S. G. Louie, Phys. Rev. B **57**, 7027 (1998).

[103] H. N. Rojas, R. W. Godby, and R. J. Needs, Phys. Rev. Lett. **74**, 1827 (1995).

[104] M. M. Rieger, L. Steinbeck, I. White, H. Rojas, and R. Godby, Comput. Phys. Commun. **117**, 211 (1999).

[105] C. Stampfl and C. V. de Walle, Phys. Rev. B **59**, 5521 (1999).

[106] L. Steinbeck, A. Rubio, L. Reining, and R. Godby, unpublished.

[107] S. Kümmel and J. P. Perdew, Phys. Rev. Lett. **90**, 043004 (2003).

[108] S. Kümmel and J. P. Perdew, Phys. Rev. B **68**, 035103 (2003).

[109] S. Kümmel, L. Kronik, and J. P. Perdew, Phys. Rev. Lett. **93**, 213002 (2004).

[110] `http://www.sfhingx.de`.

[111] M. Fuchs and M. Scheffler, Comput. Phys. Commun. **119**, 67 (1999).

[112] N. Troullier and J. L. Martins, Phys. Rev. B **43**, 1993 (1991).

[113] L. Kleinman and D. M. Bylander, Phys. Rev. Lett. **48**, 20 (1982).

[114] P. Blaha, K. Schwarz, G. K. H. Madsen, D. Kvasnicka, and J. Luitz, *WIEN2k, An Augmented Plane Wave + Local Orbitals Program for Calculating Crystal Properties*, Karlheinz Schwarz, Techn. Universität Wien, Austria, 2001.

[115] Ricardo Gómez-Abal, private communications.

[116] L. Steinbeck, A. Rubio, L. Reining, M. Torrent, I. White, and R. Godby, Comput. Phys. Commun. **125**, 105 (2000).

[117] S. Baroni and R. Resta, Phys. Rev. B **33**, 7017 (1986).

[118] P. Eggert, C. Freysoldt, P. Rinke, A. Schindlmayr, M. Scheffler, and R. W. Godby, to be published.

[119] I. D. White, R. W. Godby, M. M. Rieger, and R. J. Needs, Phys. Rev. Lett. **80**, 4265 (1997).

[120] M. Rohlfing, N.-P. Wang, P. Krüger, and J. Pollmann, Phys. Rev. Lett. **91**, 256802 (2003).

[121] G. Fratesi, G. P. Brivio, P. Rinke, and R. Godby, Phys. Rev. B **68**, 195404 (2003).

[122] G. Fratesi, G. P. Brivio, and L. G. Molinari, Phys. Rev. B **69**, 245113 (2004).

[123] O. Pulci, L. Reining, G. Onida, R. D. Sole, and F. Bechstedt, Comp. Mater. Sci. **20**, 300 (2001).

[124] P. Rinke, K. Delaney, P. García-González, and R. W. Godby, Phys. Rev. A **70**, 063201 (2004).

[125] A. Schindlmayr, Phys. Rev. B **56**, 3528 (1997).

[126] A. Qteish, J. Phys.: Condens. Matter **12**, 5639 (2000).

[127] Landolt-Börnstein, *Numerical Data and Functional Relationships in Science and Technology,* New Series, Group III, Vols. 22, Pt. a, edited by O. Madelung (Springer, Berlin, 1982).

[128] O. Madelung and Landolt-Börnstein, *Semiconductors. Intrinsic Properties of Group IV Elements and III-V, II-VI and I-VII Compounds,* New Series, Group III, Vols. 22, Pt. a (Springer, Berlin, 1982).

[129] D. R. T. Zahn, G. Kudlek, U. Rossow, A. Hoffmann, I. Broser, and W. Richter, Adv. Mater. Opt. Electron. **3**, 11 (1994).

[130] G. Ramírez-Flores, H. Navarro-Contreras, A. Lastras-Martínez, R. C. Powell, and J. E. Greene, Phys. Rev. B **50**, 8433 (1994).

[131] O. Zakharov, A. Rubio, X. Blase, M. L. Cohen, and S. G. Louie, Phys. Rev. B **50**, 10780 (1994).

[132] A. Rubio, J. L. Corkill, M. L. Cohen, E. L. Shirley, and S. G. Louie, Phys. Rev. B **48**, 11810 (1993).

[133] M. Rohlfing, P. Krüger, and J. Pollmann, Phys. Rev. B **56**, R7065 (1997).